Effects of sand-shale anisotropy on amplitude variation with angle (AVA) modelling: The Sawan Gas Field (Pakistan) as a key case-study for South Asia's sedimentary basins

Hafiz Mubbasher Anwer[1*], Tiago M. Alves[2], Aamir Ali[1], Zubair [3]

[1]Department of Earth Sciences, Quaid-i-Azam University, Islamabad, 45320, Pakistan.

[2]3D Seismic Lab, School of Earth and Ocean Sciences, Cardiff University, Main Building-Park Place, Cardiff CF10 1JZ, United Kingdom

[3]Software Integrated Solutions, Schlumberger, Pakistan.

[*] Corresponding author

Abstract

Amplitude variation with angle (AVA) is a technique widely used in the characterisation of hydrocarbon reservoirs and assumes the Earth's crust to be an isotropic medium. Yet, seismic anisotropy is known to have first-order effects on seismic AVA responses when investigating subsurface prospects. This work analyses the effects of anisotropic strata on AVA responses using the Lower Goru Formation, middle Indus basin (Pakistan) as a case-study. In the study area, shale intervals are interbedded with reservoir sands of the Sawan gas field. Shales in this gas field form laminae or are dispersed within reservoir sands, making the Lower Goru Formation an example of a vertically transversely isotropic (VTI) medium. In this work, we calculate the effective (saturated) mechanical properties of the Lower Goru Formation based on rock physics templates; the Backus (1962) average typically designed for layered media, combined with the empirical relations of Brown and Korringa (1975) and Wood (1955). The input data used in our rock physics modelling is based on a detailed petrophysical analysis of well data. Using the saturated effective mechanical properties of the Lower Goru Formation, we

generate angle-dependent reflection coefficient curves (and seismic AVA responses) based on exact and approximate solutions, for both isotropic and anisotropic reservoir scenarios. Our results suggest that the effects of lithological anisotropy are more pronounced in places with thick shale beds within reservoir sands. Conversely, angle-dependent reflection curves, and seismic AVA responses based on isotropic or anisotropic cases, give similar solutions in the presence of thin shale beds. As a corollary of this work, we present a Bayesian inversion method for the estimation of porosity in VTI media.

Keywords: South Asia; VTI medium; Rüger's approximation; PP reflection coefficients; Anisotropic AVA Modelling; Bayesian inversion.

1. Introduction

Modern techniques based on the systematic analysis of amplitude variations of seismic waves with changing distance between source and receiver (AVO), or with angle of incidence (AVA), are widely used in the petroleum industry to: a) detect subsurface gas, b) identify lithological variations, and c) analyse subsurface fluid volumes and compositions (Floridia and Teles, 1998; Grechka, 1998; Margesson and Sondergeld, 1999; Feng and Bancroft, 2006; Almutlaq and Margrave, 2010; Chao et al., 2012). Seismic AVA is of particular interest as its use is based on the realisation that variations in amplitude, at varying incident angles, result from contrasts in lithology and fluid content in rocks above and below a layer boundary (Zhang and Brown, 2001). Seismic AVA modelling is systematically carried out in reservoir studies by considering the Earth as an isotropic medium. However, all sedimentary rocks exhibit anisotropic behaviour at different scales (Xu et al., 2005). It has been known for a long time that anisotropy resulting from shaley beds and lenses within sandy successions can affect seismic AVA responses when investigating sand-shale reservoirs (Banik, 1987; Wright, 1987; Kim et al., 1993;

51 Thomsen, 1995; Blangy, 1994; Ball, 1995; Grechka, 1998; Besheli et al., 2005; Brajanovski et
52 al., 2009; Chao et al., 2012; Nourollah et al., 2015). By ignoring the effects of anisotropy during
53 AVA modelling, interpreters may complete erroneous characterisations of productive reservoir
54 intervals (Besheli et al., 2005). Importantly, erroneous quantification of volumes and reservoir
55 distribution(s) should arise when analysing the petroleum potential of sedimentary basins in
56 South Asia, and other parts of the world, where stratified reservoir sequences of shale and silt
57 contain significant amounts of 'tight oil' and 'tight gas' (McGlade et al., 2012; Katz and Lin,
58 2014; English et al., 2015; Rodriguez et al., 2016).

59 In recent decades, stratigraphic sequences of thin-layered sands and shales have become
60 key exploration targets for which seismic anisotropy methods (also referred to as long-
61 wavelength anisotropy) are useful and broadly successful in their characterisation (Crampin et
62 al., 1984; Sayers, 2013; Sone and Zoback, 2013; Das and Zoback, 2013). Shale layers within a
63 horizontally-bedded sand matrix behave elastically as transversely isotropic (TI) media, i.e. they
64 have similar wave properties in two perpendicular directions, but are significantly different in a
65 third orthogonal direction (Sone and Zoback, 2013). In these same sequences, vertical axes of
66 symmetry are often described as vertically transversely isotropic (VTI) media (da Silva et al.,
67 2016; Li et al., 2016).

68 The anisotropic behaviour of VTI media is usually quantified by using Thomsen's
69 anisotropic parameters ε, δ, γ (Thomsen, 1986), in which ε denotes the fractional difference
70 between the horizontal and vertical P-wave velocities, δ describes the variation in P-wave
71 velocity with phase angle for near-vertical propagation, and γ denotes the fractional difference
72 between the horizontal and vertical SH-wave velocity (Rüger, 2002). The empirical forms of ε,
73 δ, γ are provided by Rüger (2002) as:

74

75 $$\gamma = \frac{C_{66} - C_{55}}{2C_{55}}, \qquad (1)$$

$$\varepsilon = \frac{C_{11} - C_{33}}{2C_{33}}, \tag{2}$$

and

$$\delta = \frac{(C_{13} + C_{55})^2 - (C_{33} - C_{55})^2}{2C_{33}(C_{33} - C_{55})}. \tag{3}$$

Here, C represents the stiffness and its indices denote standard constants for VTI media. In essence, elastic anisotropy in VTI media can be characterised by five independent elastic constants, which can be expressed in two notations: a) in terms of stiffness constants ($C_{11}, C_{13}, C_{33}, C_{55}$ & C_{66}), or b) in terms of vertical velocities (V_P and V_S) and Thomsen's anisotropic parameters ($\varepsilon, \delta, \gamma$) (Tsvankin, 1997a, 1997b). These five independent elastic constants are very difficult to apply to AVA analyses, and most of these latter are developed by assuming a non-VTI medium.

Several researchers have attempted to estimate seismic anisotropy and incorporate it into AVA-based methods using seismic, VSP, well logs and core data (Blangy, 1992, Leaney, 1993; Blangy, 1994, Margesson and Sondergeld, 1999; Besheli et al., 2005, Luo et al., 2005, Wang et al., 2006; Brajanovski et al., 2009; Goodway et al., 2010; Wang, 2011), but seldom for hydrocarbon-rich basins in South Asia. However, in the Indian subcontinent (including Pakistan and bordering countries), important tight oil and gas reservoirs have been found in the hinterland basins that surround the Himalayan and Baluchistan mountain ranges. The Indus basin is currently the main focus of oil and gas exploration and production in Pakistan (Alam et al., 2014; Asim et al., 2015) (Figure 1a). In this basin, as in other hydrocarbon-productive regions of South and Southeast Asia, the successful use of AVA techniques in reservoir characterisation is critically dependent upon the careful estimation of the anisotropic parameters of sedimentary rocks (Zaigham and Mallick, 2000; Chengzao et al., 2012; Zhu et al., 2012; Jinhu et al., 2014).

In this work, we use well log data from the Sawan gas field (Figure 1b), middle Indus basin (Pakistan), to focus on the Cretaceous Lower Goru C-sand reservoir, which is interbedded with shales. We use reservoir properties estimated from borehole data as key data inputs to our rock physics models, and to later carry out anisotropic and isotropic AVA analyses. Rock physics models are often used to link seismic data to reservoir properties (Avseth et al., 2005). Seismic-based estimates of reservoir properties can be uncertain, but the inclusion of rock physics models in exploration workflows is, nevertheless, capable of reducing the level of uncertainty by decreasing the number of unknown parameters in AVA analyses. In other words, rock physics modelling represents a type of regularization within the context of seismic inversion (Ali and Jakobsen, 2011a, 2011b).

The aim of this work is to analyse the effects of anisotropy generated by interbedded shales within the reservoir sands, and its implications to AVA-based reservoir studies. In parallel, we investigate how accurate are seismic AVA methods for both exact (Zoeppritz, 1919; Daley and Horn, 1977) and approximate (Rüger, 1998; 2002) solutions for PP-reflection coefficients within the context of isotropic and anisotropic cases.

2. Geological setting

The Sawan gas field lies in the middle Indus basin, in the eastern border of Pakistan (Zaigham and Mallick, 2000). The study area is bounded by the Sargodha High to the north, and by the Jacobabad and Mari-Kandkot Highs to the south (Figure 1a). The Indian Shield bounds the eastern side of the study area, whereas the Kirthar and Suleiman fold-and-thrust belts mark its western boundary (Kadri, 1995; Afzal et al., 2009). Regional geological data indicate that the structural evolution of the Sawan gas field was closely controlled by three post-rift tectonic events: a) Late Cretaceous uplift and erosion, b) NW–trending thick-skinned wrench faulting and c) Late Tertiary to present-day tectonic uplift of the Jacobabad and Khairpur Highs (Ahmad et

al., 2004; Afzal et al., 2009; Azeem et al., 2016). These latter structural highs played an important role in the formation of structural and stratigraphic traps, not only in the Sawan area, but also in multiple oil and gas fields in the region (Ahmad et al., 2004; Fink et al., 2004; Berger et al., 2009).

Cretaceous black shales in the Sembar Formation are the proven source rock in the middle and lower Indus basins, which were mainly filled with shale and minor amounts of black siltstone, sandstone and nodular argillaceous limestone (Quadri and Shuaib, 1986; Kadri, 1995). The thickness of the Sembar Formation ranges from 0 m to more than 260 m (Iqbal and Shah, 1980). The Sembar Formation is deeply buried and matures thermally towards the western edge of the Indus basin. It becomes shallower and less mature towards its eastern edge (Wandrey et al., 2004). In the study area, the tectonic uplift recorded by the Khairpur High controlled the depositional patterns of the main reservoir unit (Goru Formation); reservoir sands in proximal depositional systems are positioned in structurally deep areas, whereas non-reservoir distal shales are positioned up-dip to form major structural traps (Azeem et al., 2016, Berger et al., 2009). The depositional environment of the Lower Goru Member, which comprises the main reservoir interval above the Sembar Formation, was marine and reflects deposition at the western (passive) margin of the Indian plate.

The Sembar Formation is, therefore, overlain by the Lower Goru Member of the Goru Formation, i.e. the proven reservoir interval in the Sawan gas field (Fig. 2). The upper part of the Lower Goru Member is chiefly composed of shales, whereas its lower part comprises medium to coarse-grained sandstones with thin layers of shale and limestone. The lower portion of the reservoir interval can be subdivided into distinct sand intervals: A, B, C and D (Krois et al., 1998) (Figure 2). The deposition of these sand intervals took place in deltaic, shallow-marine environments during sea-level lowstands, when medium to coarse-grained sediment was deposited on top of the distal (shale and siltstone) strata of previous highstand systems tracts (HSTs) (Berger et al., 2009, Azeem et al., 2016).

Petrographically, intervals A and B can be classified as quartz-rich arenites (Berger et al., 2009). The C interval includes significant amounts of partially altered volcanic rock fragments and pore lining iron chlorite cement. Thus, the sands of interval C can be classified as sublithic to lithic arenites (McPhee and Enzendorfer, 2004; Berger et al., 2009; Azeem et al., 2016). Sands in the B and C intervals comprise the main gas reservoirs in the study area (Munir et al., 2011), showing high porosity (i.e. around 16 %) and permeability at depths between 3000–3500 m (Azeem et al., 2016). These two reservoir intervals of the Lower Goru Member are draped by transgressive shales and siltstones of the Upper Goru Member, which acts as a regional seal in the middle and lower Indus basins (Berger et al., 2009).

3. Dataset and methods

Data from three exploration wells (Sawan-01, Sawan-3B and Sawan-06) are used in this study to analyse the acoustic effects of the lithologic anisotropy created by interbedded shales in the C-sand reservoir. The rationale behind selecting the Sawan gas field as a case study results from the fact that it is located in the tectonically stable part of the Thar Platform, in the middle Indus basin. It also shows marked alternations of sands and shales, being a typical example of a VTI medium.

The workflow adopted in this work is shown in Figure 3. In a first instance, we analysed sand-shale distribution patterns in the main reservoir intervals using the methodology proposed by Thomas and Stieber (1975). In a second stage, rock physics modelling was undertaken using the Backus (1962) approach for dry composite porous media (sand-shale), used together with the relationships of Brown and Korringa (1975) and Wood (1955). These latter relationships allowed us to incorporate fluid effects on the mechanical properties of strata. The aim of the second stage of our analysis was to obtain (saturated) effective elastic properties for the Lower Goru reservoir

intervals (see also Jakobsen et al., 2003a, 2003b; Ali and Jakobsen, 2011a, 2011b; Ali et al., 2016).

In a third stage exact solutions of P-wave reflection coefficients, derived from Zoeppritz (1919) solutions for isotropic media and Daley and Horn's (1977) solutions for VTI media, were used to generate angle dependent reflection coefficients and seismic AVA data from the top of the reservoir, for both isotropic and anisotropic cases. In parallel, the Rüger's approximation (Rüger, 1998, 2002) was used for angle dependent reflection coefficients and seismic AVA data from the top of the reservoir, for both isotropic and anisotropic cases, over the Sawan reservoir intervals. Finally, a Bayesian inversion scheme was utilised to investigate the implications of isotropic and anisotropic AVA solutions on the estimation of porosity throughout the reservoir.

3.1 Sand-Shale distribution analysis

To understand shale distribution within reservoir sands is an integral part of forward modelling using rock physics templates (Ali et al., 2016). Prior to developing the appropriate rock physics model for AVA modelling, sand-shale distribution analyses are necessary to identify the type of shale(s) distributed within reservoir sands (Ali et al., 2016). This step improves confidence in the interpretation of sand-shale reservoirs because it helps interpreters to decide which geophysical approach is appropriate for a particular reservoir (Kurniawan, 2005). The distribution of shale within reservoir sands has a pronounced effect on reservoir production performance due to decreasing porosity values and variable saturations that derive from the presence of shales (Sames and Adrea, 2001; Ali et al., 2016). Hence, sand-shale distribution analyses require robust stratigraphic correlations based on gamma-ray log data (Figure 4). Gamma-ray curves are particularly helpful in the identification of shales within reservoir sand, and for detailed petrophysical analyses and correlations. The petrophysical interpretation of wells

(Sawan-01, Sawan-3B and Sawan-06) was carried out to determine key reservoir properties such as P-wave velocity (V_p), S-wave velocity (V_s), porosity (ϕ), density (ρ), volume of shale (V_{sh}) and water saturation (S_w) for the C-sand of the Lower Goru Member (Figures 5-7). The details of estimated reservoir parameters are given in Tables 1-3.

The parameters commonly required in sand-shale distribution analyses are volume of shale, porosity and water saturation, with the volume of shale being a critical parameter that controls the two latter (Saxena et al., 2006). Once these parameters are estimated, the Thomas-Stieber (1975) method in Figure 8 can be used to estimate shale distribution patterns (Saxena et al., 2006). The Thomas-Stieber (1975) method estimates shale distribution utilizing a cross-plot with volume of shale along the X-axis and total porosity along the Y-axis. The position of data points on the cross-plot allows the identification of the type(s) of shale distribution within sands.

Usually, shales are distributed through four different ways within sands: a) as laminae, b) through structures (faults, joints), c) dispersed in sands, and d) as any combinations of the three latter ways (Clavaud et al., 2005; Sams and Andrea, 2001). The results from sand-shale analyses undertaken for the three studied wells suggest that, in our study area, laminar and dispersed shales are distributed within reservoir sands (Figures 9-11).

3.2. Forward Modelling

The nonlinear forward problem is defined as:

$$\mathbf{d} = \mathrm{G}(\mathbf{m}). \qquad (4)$$

In Equation (4), $\mathbf{d}$ is a vector of observable quantities (angle-dependent reflection coefficients or seismic AVA data) and $\mathbf{m}$ is a vector of model parameters required to be estimated over the

model space **M** i.e.$\mathbf{m} \in \mathbf{M}$. The operator G is a forward modelling operator used for generating synthetic angle-dependent reflection coefficients, or seismic AVA data, via rock physics and seismic modelling. In the subsequent section we will discuss the rock physics modelling for a layered medium.

3.2.1 Rock Physics modelling

Rock physics models are important to correlate variations in reservoir properties (lithology, porosity, permeability, pore fluid, etc.) with changes in the velocities (V_p, V_s) and density (ρ) observed on well data (Uden et al., 2004). Rock physics models act as a bridge between geological properties (reservoir parameters) and geophysical data by upscaling the reservoir variables related to lithology, shale content and fluid parameters (Bachrach, 2006; Avseth et al., 2005). Rock physics also provide a realistic and systematic basis for seismic-attribute generation and interpretation (Avseth et al., 2005). In clastic reservoirs, shales are often found to behave elastically as transversely isotropic media with a vertical axis of symmetry (Jakobsen and Johansen, 1999, 2000). In forward models, rock physics models are used to calculate effective elastic properties from petrophysical properties estimated from wireline-log data.

Results of shale distribution analyses within the Sawan gas field reservoir sands show that laminar and dispersed shale types are distributed in the host medium. Such a medium can be modelled using anisotropic rock physics (Ali et al., 2016; Ali et al., 2015; Jakobsen et al., 2003; Sayers and Rickett 1997; Sayers, 1998; Backus, 1962). In this study, we follow the approach given by Backus (1962), which was typically designed for a layered medium (see Appendix-A). The fluid effects are incorporated via the Gassmann model for isotropic cases and via the Brown and Korringa (1975) model for anisotropic cases, in conjunction with the Wood (1955) model for homogenous saturations (Appendix-B).

3.2.2 Seismic amplitude variation with angle (AVA) modelling

Seismic AVA modelling is considered to be the most effective technique for reservoir characterisation. In practice, AVA studies are the method most widely used for gas detection, lithology identification and fluid parameter analyses (Feng and Bancroft, 2006). Seismic response of variations in effective elastic properties obtained through rock physics tools for sand-shale layers can be modelled using synthetic seismic AVA data. From the effective elastic properties as calculated above, angle-dependent reflection coefficients and seismic AVA data can be generated using the exact Zoeppritz (1919) formulation for isotropic media, and the Daley and Horn's (1977) exact methods for anisotropic (VTI) media. We also tested the Rüger (2002) approximation for the generation of reflection coefficients for both isotropic and VTI media. The rationale behind only selecting Rüger's approximation for isotropic and VTI media is that the Rüger's technique is only linearised in terms of small contrasts in medium parameters, without having any additional assumption on Poisson's or V_p/V_s ratios (Rüger, 2002).

3.2.2.1 P-wave reflection coefficient for isotropic media

The exact Zoeppritz (1919) empirical relation (see Equation 5) allows us to calculate the PP-wave reflection coefficients (R_{PP}) of a rock as a function of the incidence angle from the top of an isotropic medium, which can be represented as a system of linear equations given as (Pujol, 2003):

$$A\boldsymbol{X} = B, \tag{5}$$

Where:

$$A = \begin{bmatrix} -Sine & Cosf & Sine' & Cosf' \\ Cose & \sin f & \cos e' & -Sinf' \\ Sin\,2e & -\frac{\alpha}{\beta}Cos\,2f & \frac{\rho'\alpha}{\rho\alpha}\left(\frac{\beta'}{\beta}\right)^2 Sin\,2e' & \frac{\rho'\alpha}{\rho\beta'}\left(\frac{\beta'}{\beta}\right)^2 Cos\,2f' \\ -Cos\,2f & -\frac{\beta}{\alpha}Sin\,2f & \frac{\rho'\alpha}{\rho\alpha}Cos\,2f' & -\frac{\rho'\beta'}{\rho\alpha}Sin\,2f' \end{bmatrix}, \quad (6)$$

$$\boldsymbol{X} = \begin{bmatrix} R_{PP} \\ T_{PP} \\ R_{PS} \\ T_{PS} \end{bmatrix}, \quad (7)$$

$$\text{and } B = \begin{bmatrix} Sine \\ Cose \\ Sin\,2e \\ Cos\,2f \end{bmatrix}. \quad (8)$$

The unknown vector $\boldsymbol{X}$ can be obtained by:

$$\boldsymbol{X} = A^{-1}B. \quad (9)$$

In these equations, α, β, ρ, e and f are the P-wave velocity, S-wave velocity, density, P-wave transmission angle, and SV–wave transmission angle of the upper half space. Conversely, α´, β´, ρ´, e´ and f´ are the P-wave velocity, S-wave velocity, density and P-wave reflection angle, and SV–wave reflection angle of the lower half space.

3.2.2.2 Formulation of PP-wave reflection coefficients for VTI media

The exact algebraic solution for reflection/transmission coefficients (R, T) of plane incident P-waves in a VTI medium, developed by Daley and Horn (1977), is used in this work. The concise form of the exact solution of P-wave reflection coefficients for a VTI medium (R_{PP}^{VTI}), in matrix form, is given below (Graebner, 1992; Rüger, 2002):

$$M\boldsymbol{R} = b, \quad (10)$$

where $\boldsymbol{b} = [-m_{11}, -m_{21}, m_{31}, m_{41}]^T$, (11)

and $\boldsymbol{R} = \begin{bmatrix} R_{PP}^{VTI} \\ R_{PS}^{VTI} \\ T_{PP}^{VTI} \\ T_{PS}^{VTI} \end{bmatrix}$. (12)

By using Cramer's rule, the solution for unknown vector $\boldsymbol{R}$ can be expressed in its analytic form as:

$$\boldsymbol{R} = \frac{1}{\det \mathrm{M}} \begin{bmatrix} M_{11} & M_{12} & M_{13} & M_{14} \\ M_{21} & M_{22} & M_{23} & M_{24} \\ M_{31} & M_{32} & M_{33} & M_{34} \\ M_{41} & M_{42} & M_{43} & M_{44} \end{bmatrix}^T \boldsymbol{b}. \quad (13)$$

The values of matrices M and $\boldsymbol{b}$ are given by Rüger (2002), Graebner (1992) and Daley and Horn (1977).

3.2.2.3 Approximations for P-wave reflection coefficients

We also investigate the accuracy of Rüger's (2002) approximation for both isotropic and VTI media with the exact solutions given by Zeoppritz's (1919) and Daley and Horn's (1977). Rüger's approximation for isotropic media is given below (Rüger, 2002):

$$\mathrm{R}_{\mathrm{PP}}^{\mathrm{iso}}(i) = \frac{1}{2}\frac{\Delta \mathrm{Z}}{\overline{\mathrm{Z}}} + \frac{1}{2}\left\{\frac{\Delta \mathrm{V_{P0}}}{\overline{\mathrm{V}}_{\mathrm{P0}}} - \left(\frac{2\overline{\mathrm{V}}_{\mathrm{S0}}}{\overline{\mathrm{V}}_{\mathrm{P0}}}\right)^2 \frac{\Delta \mathrm{G}}{\overline{\mathrm{G}}}\right\} \sin^2 i + \frac{1}{2}\left\{\frac{\Delta \mathrm{V_{P0}}}{\overline{\mathrm{V}}_{\mathrm{P0}}}\right\} \sin^2 i \tan^2 i. \quad (14)$$

Where Z is the P-wave impedance, G is the shear wave modulus, V_{P0} is the vertical P-wave velocity, and V_{S0} is the vertical shear-wave velocity. The character delta (Δ) stands for contrasts across an interface ($\Delta Z = Z_2 - Z_1$), and the bar over a symbol represents its average ($\overline{Z} = \frac{Z_1+Z_2}{2}$). Subscript 1 corresponds to the upper layer and subscript 2 denotes the lower layer. Rüger's approximation for the generation of reflection coefficients as a function of incidence angle (i), in the case of VTI media (Rüger, 2002), is written as:

$$R_{PP}^{VTI}(i) = \frac{1}{2}\frac{\Delta Z}{\overline{Z}} + \frac{1}{2}\left\{\frac{\Delta V_{P0}}{\overline{V}_{P0}} - \left(\frac{2\overline{V}_{S0}}{\overline{V}_{P0}}\right)^2 \frac{\Delta G}{\overline{G}} + \Delta\delta\right\}\sin^2 i + \frac{1}{2}\left\{\frac{\Delta V_{P0}}{\overline{V}_{P0}} + \Delta\varepsilon\right\}\sin^2 i \tan^2 i. \quad (15)$$

The additional terms ε and δ are Thomsen's (1985, 1996) anisotropy parameters for VTI media.

3.3 Inverse modelling

In Bayesian settings, the solution of the inverse problem is given by the posterior probability distribution $q(\mathbf{m}\,|\,\mathbf{d})$ applied over the model space M. In essence, $q(\mathbf{m}\,|\,\mathbf{d})$ carries all the information about the model originating from the likelihood $L(\mathbf{m})$ and *a priori* probability density function $p(\mathbf{m})$. Bayes' theorem allows to relate $q(\mathbf{m}\,|\,\mathbf{d})$ with $L(\mathbf{m})$ and $p(\mathbf{m})$ given as (Aster et al., 2005):

$$q(\mathbf{m}\,|\,\mathbf{d}) \propto L(\mathbf{m})p(\mathbf{m}). \quad (16)$$

Here $\propto$ is the sign of proportionality. The solution of the posterior distribution can be written in a compact form as (Aster et al., 2005; Tarantola, 2005):

$$q(\mathbf{m} \mid \mathbf{d}) = N.\, e^{-J(\mathbf{m})}, \tag{17}$$

where N is the normalization constant. The functional form of the objective function $J(\mathbf{m})$, required to be minimised in the case of Gaussian statistics, and an uninformative prior distribution, is given by Aster at al., (2005) as:

$$J(\mathbf{m}) = \min \sum_{i=1}^{n} \frac{\left((G(\mathbf{m}))_i - d_i\right)^2}{2\sigma^2}. \tag{18}$$

Here, σ is the standard deviation of the measured seismic data. The rationale behind assuming an uninformative prior distribution is that we do not intend to constrain our inversion scheme by incorporating *a priori* information (obtained mostly from log/core/laboratory data) about the model parameters. There are different methods available for the evaluation of $q(\mathbf{m} \mid \mathbf{d})$, most of which are described in Ali et al. (2011a; 2011b and 2015).

4. Numerical results and discussion

In this work, we analyse the effects created by sand-shale anisotropy on AVA response with the help of rock physics modelling. In parallel, we present a comparison of exact and approximate AVA solutions for isotropic and anisotropic scenarios. Before applying rock physics modelling to layered media, it is very important to identify the type of shale distribution within reservoir sands, e.g. laminar, structural, dispersed, and so on. For this same purpose, we followed the approach presented in Section 3.1 for the C-sand reservoir unit (Lower Goru Member) drilled by

wells Sawan-01, Sawan-3B and Sawan-06. Reservoir properties are estimated through petrophysical analyses of well log data acquired in the Sawan field and results are presented in Figures 5-7 and in Tables 1-2.

The analysis of shale distribution suggests that the C-sand comprises laminated and dispersed shale types (Figures 8-11). Thus, the Lower Goru C-sand may be a potential candidate to be characterised as a VTI medium, rather than isotropic. Laminar shales in the C-sand reservoir comprise thin layers of allogenic clays and do not control effective porosity, water saturation, or the horizontal permeability of rock. However, they significantly change vertical permeability (Kurniawan, 2005). Each lamina differs in thickness, in a way that the amounts of sand, silt and clay in the layer are repeated as depositional sequences (or cycles) under dual flow regimes that denote contrasts in energy level.

The saturated effective elastic properties for isotropic and VTI media are obtained using the methodology discussed in section 3.2. The input to our rock physics modelling, in the form of elastic and reservoir properties of the Lower Goru C-sand, intra-reservoir shale layers and overburden strata, is extracted from the petrophysical analyses summarised in Table 3. The elastic properties of solid mineral (quartz) and fluid (water and gas), required to generate AVA data, are given in Table 4.

For the generation of isotropic angle-dependent reflection coefficient curves are used the exact solution of Zeoppritz (1919) for isotropic media, and Daley and Horn's (1977) solution for VTI media. Rüger's (2002) approximation is also used for both isotropic and VTI media to investigate the accuracy of exact and approximate solution of P-wave reflection coefficients as a function of incidence angle.

The angle dependent reflection coefficient (RC) curves are key to explain the main results in this work. We demonstrate in Figs. 12-14 that the intercept (normal incidence i.e. zero offset, P-wave reflectivity) and slope of the curve (gradient) indicate how the amplitude of RC changes with angle/offset. The gradient of each RC curve is almost the same, but there are small

differences in the magnitude of angle-dependent PP-reflection coefficients when comparing the isotropic and anisotropic cases (Figures 12-14). If we examine variations in RC based upon isotropy and anisotropy it is obvious that, in the Sawan-01 well, only small differences can be observed between isotropic and anisotropic RC curves (Figure 12). This clearly demonstrates that strata drilled in Sawan-01 have a weak anisotropy ($\varepsilon = 0.0214$, $\delta = 0.0306$, $\gamma = 0.0186$). In Sawan-3B, there are insignificant variations between isotropic and anisotropic RC curves (Figure 13). Finally, for Sawan-06 there is a significant variation in RC curves when comparing the isotropic and anisotropic cases (Figure 14). More importantly, if we relate these variations in RC curves with varying shale content, we can conclude that the wells with comparatively thick shale layers show substantial variations between their isotropic and anisotropic RC curves. The best example is, naturally, the RC response documented in well Sawan-06 (Figure 14; see also thick shale content marked in yellow in Figure 4).

We observe that AVA data is moderately sensitive to the anisotropy of the medium. In essence, our results confirm that little or no effects created by anisotropy upon reflection curves are diagnostic of very weakly anisotropic media. Significantly, as shales are strongly anisotropic and heterogeneous (Kumar et al., 2012), exploration well(s) that encountered thick shale layers in the study area show clear variations between the behaviour of isotropic and anisotropic angle dependent PP-reflection coefficients (Figure 14). Based on data from the three interpreted wells (Sawan-01, Sawan-3B and Sawan-06), shale anisotropy increases proportionally to shale content, and the effect of this same shale anisotropy upon reflection curves becomes more pronounced. As such, it is advisable to predict anisotropy in a medium during AVA studies, especially when thick allogenic shale layers are present in reservoir successions.

The investigation of Rüger (2002) approximation's accuracy for both isotropic and VTI media reveal that the predicted magnitude of reflection coefficients is significantly different in all the three studied wells, at large offsets. Also, the gradient predicted by the Rüger (2002) approximation is high when compared to the exact solutions.

411 For seismic AVA response in isotropic and VTI media, angle-dependent reflection
412 coefficients are convolved with the source (Ricker) wavelet (Figures 15-17). It can be observed
413 from our approach that the amplitude of synthetic AVA gathers show a decreasing trend with
414 increasing angle of incidence. The difference between exact and approximate solutions is more
415 pronounced in the magnitude of predicted seismic AVA amplitude values (Figures 15-17).
416 The AVA response of VTI media is sensitive to contrasts in Thomsen's anisotropic
417 parameters, ε and δ, across the interface (Blangy 1994; Margesson and Sondergeld, 1999). As
418 also identified by Daley and Horn (1977), generally P-P reflections indicate that the smaller the
419 contrast in isotropic properties (V_P, V_s, ρ), and the larger the contrast in δ (variation in P-wave
420 velocity with phase angle for near vertical propagation) across a reflection interface, the greater
421 are the effects of anisotropy on AVA signatures. Contrasts in δ are most important under small-
422 to-medium angles of incidence, as previously reported in Banik (1987), whereas contrasts in ε
423 (fractional difference between the horizontal and vertical P-wave velocities) can have a strong
424 influence on amplitudes for the larger angles of incidence (21^o) commonly used in exploration
425 seismic data. The increasing trend in gradients is more pronounced at far offsets (21^o to 40^o),
426 revealing an increasing sensitivity in terms of anisotropy and isotropy with increasing offset
427 angles.
428 The AVA modelling also proves a strong relationship between porosity and reflection
429 coefficient for all offset ranges. Therefore, in order to check the accuracy of exact and
430 approximate solutions for P-wave reflection coefficients in AVA inversion, we tried to recover
431 true reservoir porosity distribution (with 20% uncertainty) under the Bayesian settings discussed
432 in Section 6. For this purpose, a correlated Gaussian field was generated representing the true
433 porosity (Buland and Omre, 2003) distribution throughout the reservoir within 100×100 grid
434 blocks (Figure 18). Later, a AVA modelling approach (exact/approximate VTI or
435 exact/approximate isotropic) was performed using a maximum-a-posteriori (MAP) solution. The

results suggest that the exact VTI solution recovers the porosity trends with much more accuracy when compared to all other solutions, under significant noise conditions (Figure 18).

5. Conclusions

In industry, seismic AVA/AVO techniques are being increasingly used for amplitude-based reservoir characterisation, but frequently assume that subsurface media are isotropic. Seismic anisotropy is known to have a first order effect on AVA modelling but this effect is often ignored during AVA studies, providing significant errors when describing reservoir intervals. In this work we analyse the effects of anisotropy on AVA modelling and inversion for a sand-shale reservoir in the Sawan gas field, Pakistan. The main conclusions of this work are as follows:

a) AVA modelling shows that anisotropy effects are more pronounced in stratigraphic intervals where interbedded shales are relatively thick within reservoir sand (Sawan-06 well). The exact/approximate isotropic or VTI solutions show smaller variations in the presence of thin interbedded shale layers within reservoir sands.

b) The exact solution for VTI media provided by Daley and Horn's (1977) is one with the highest potential for performing AVA inversion in sand-shale media with weak to strong anisotropy. We have demonstrated this fact by completing a numerical synthetic experiment for recovering porosity distributions through the Lower Goru reservoir.

c) The choice of approximate solution(s) for AVA modelling is crucial in any workflow since, in most cases, there is a significant difference in the predictions of magnitude of reflection coefficients, and gradient of the reflection curves, resulting from distinct approximate solutions. As suggested by our own AVA modelling results, the Rüger's approximation is significantly different to other techniques when considering the magnitude and gradient of reflection curves. This fact can create additional uncertainty to the use of AVA inversion techniques in the characterisation of shale-sand reservoirs.

Acknowledgments

Dr. Aamir Ali (Advisor) and Hafiz Mubasher Anwer (PhD Scholar) would like to thank the Higher Education Commission (HEC) of Pakistan for providing the necessary funding needed to complete this research work. The authors are also pleased to the Director General Petroleum Concessions (DGPC), Ministry of Petroleum and Natural Resources, Government of Pakistan and joint venture partners of Sawan gas field for providing data and other required material to complete this work. TA thanks Cardiff University for their support to a visiting staff scheme set with HMA. Reviewers and Editor M. Faure are acknowledged for their constructive feedback.

References

Afzal, J., Kuffner, T., Rahman, A., Ibrahim, M., 2009. Seismic and well-log based sequence stratigraphy of the early Cretaceous, Lower Goru "C" sand of the Sawan gas field, middle Indus Platform, Pakistan. Annual Technical Conference, Islamabad.

Ahmad, N., Fink, P., Sturrock, S., Mahmood, T., Ibrahim, M., 2004. Sequence stratigraphy as predictive tool in Lower Goru fairway, Lower Middle Indus Platform, Pakistan. PAPG-SPE ATC, 85-105.

Alam, I., Azhar, A.M., Khan, M.W., 2014. Frontal structural style of the Khisor Range, northwest of Bilot: Implications for hydrocarbon potential of the north-western Punjab foredeep, Pakistan. Journal of Himalayan Earth Sciences, Volume 47, Issue No. 1, 87-98.

Ali, A., Anwer, H.M., Hussain, M., 2015. A comparisonal study in the context of seismic fracture characterization based on effective stiffness and compliance methods, Arab. J. of Geosci., DOI :10.1007/s12517-014-1478-8

485 Ali, A., Jakobsen, M., 2011a. On the accuracy of Rüger's approximation for reflection
486 coefficients in HTI media: implications for the determination of fracture density and orientation
487 from seismic AVAZ data. Journal of Geophysics and Engineering, issue No. 8, 372-393.

488 Ali, A., Jakobsen, M., 2011b. Seismic characterization of reservoirs with multiple fractures sets
489 using velocity and attenuation anisotropy data, Journal of Applied Geophysics, Issue No.75, 590-
490 602.

491 Ali, A., Shahraini, A., Jakobsen, M., 2011. Improved characterization of fault zones by
492 quantitative integration of seismic and production data, Journal of Geophysics& Eng. Issue 8,
493 259–274.

494 Ali, A., Zubair, Hussain, M., Rehman, K., Toqeer, M., 2016. Effect of Shale Distribution on
495 Hydrocarbon Sands Integrated with Anisotropic Rock Physics for AVA Modelling: A Case
496 Study, Acta Geophysica, vol. 64, issue No. 4, 1139-1163.

497 Almutlaq, M.H., Margrave, G.F., 2010. Tutorial: AVO inversion, CREWES Research Report,
498 Vol. 22, 1-23.

499 Asim, S., Zhu, P., Qureshi S.N., Naseer, M.T., 2015. A case study of Precambrian to Eocene
500 sediments' hydrocarbon potential assessment in Central Indus Basin of Pakistan, Arabian Journal
501 of Geosciences, ISSN 1866-7511, DOI 10.1007/s12517-015-1988-z.

502 Aster, R.C., Borchers, B., Thurber, C.H., 2005. Parameter Estimation and Inverse Problems.
503 ISBN: 0-12-065604-3, Elsevier Academic Press, Amsterdam.

504 Avseth, P., Mukerji, T., Mavko, G., 2005. Quantitative seismic interpretation: Applying rock
505 physics tools to reduce interpretation risk. ISBN: 0-13-978-0-521-81601-7, Cambridge
506 University Press, UK.

507 Azeem, T., Yanchun, W., Khalid, P., Xueqing, L., Yuan, F., Lifang, C., 2016. An application of
508 seismic attributes analysis for mapping of gas bearing sand zones in the Sawan gas field Pakistan.
509 Acta Geod. Geophys, DOI 10.1007/s40328-015-0155-z.

510 Bachrach, R., 2006. Joint estimation of porosity and saturation using stochastic rock-physics
511 modelling. Geophysics, 71(5), 53–63.

512 Backus, G.E.,1962. Long-wave elastic anisotropy produced by horizontal layering. J.
513 Geophysics, Res., issue No.67, 4427-4440.

514 Ball, G., 1995. Estimation of anisotropy and anisotropic 3-D Prestack depth migration, offshore
515 Zaire. Geophysics, issue No. 60, 1495-1513.

516 Banik, N. C., 1987. An effective anisotropy parameter in transversely isotropic media.
517 Geophysics, 52(12), 1654-1664.

518 Berger, A., Gier, S., Krois, P., 2009. Porosity-preserving chlorite cements in shallow-marine
519 volcaniclastic sandstones: evidence of the Sawan gas field Pakistan. AAPG Bull 93(5), 595-615.

520 Besheli, S. A., Urosevic, M., Li, R., 2005. The effect of seismic anisotropy on reservoir
521 characterization. SEG Annual Meeting Houston, USA.

522 Blangy, J.P.,1992. Anisotropy and AVO in TI media, an overview: Joint SEG. In EAEG summer
523 research workshop, Expanded Abstracts, Vol. 60, l-605.

524 Blangy, J.P.,1994. AVO in transversely isotropic media-An overview, Geophysics, Vol 59, No.5,
525 775-781.

526 Brajanovski, M., Nadri, D., Gurevich, B. Bona, A., 2009. Stress induced anisotropy in sandstone
527 reservoir and shale overburden - AVO modeling. International Geophysical Conference and

528 Exposition, Beijing, China, 24–27 April, 194-194. ISBN: 978-1-56080-284-6 doi:
529 10.1190/1.3603719.

530 Brown, R.J.S., Korringa, J., 1975. On the dependence of elastic properties of a porous rock on
531 the compressibility of the pore fluid. Geophysics 40, 608–616.

532 Buland, A., Omre, H., 2003. Joint AVO inversion-wavelet estimation and noise level estimation
533 using a spatially coupled and hierarchical Bayesian Model, Geophysical Prospecting, 51, 531-
534 550.

535 Chao G., Cadore, T., Deplante, C., Gratzer, O., 2012. Detailed AVA analysis of a class IIp
536 reservoir in presence of VTI shale anisotropy. A case study from offshore West Africa. SEG
537 Annual Meeting, Las Vegas, DOI:10.1190/segam2012-1280.1.

538 Chengzao, J., Min, Z., Yongfeng, Z., 2012. Unconventional Hydrocarbon Resources in China
539 and the Prospect of Exploration and Development. Petroleum Exploration and Development, v.
540 39/2, 129-136.

541 Clavaud, J.B., Nelson, R., Guru, U.K., Wang, H., 2005. Field example of enhanced hydrocarbon
542 estimation in thinly laminated formation with a triaxial array induction tool: A laminated sand-
543 shale analysis with anisotropic shale. SPWLA 46th Annual Logging Symposium, 26-29 June,
544 New Orleans, USA.

545 Crampin, S., Chesnokov, E.M., Hipkin, R.G., 1984. Seismic Anisotropy- the state of the art: II.
546 Geophysics. J. Int. issue 76(1), 1-16.

547 Da Silva, N.V., Ratcliffe, A., Vinje, V., Conroy, G., 2016. A new parameter set for anisotropic
548 multiparameter full-waveform inversion and application to a North Sea dataset. Geophysics, Vol.
549 81, issue No. 4, U25–U38.

550 Daley, P.F., Horn, F., 1977. Reflection and transmission coefficients for transversely isotropic
551 media. Bull. Seis. Soc. Am., issue No. 67, 661-675.

552 Das, I., Zoback, M.D., 2013. Long-period, long-duration seismic events during hydraulic
553 stimulation of shale and tight-gas reservoirs Part 1: Waveform characteristics. Geophysics, Vol.
554 78, No. 6, KS97-KS108.

555 English, J.M., Lunn, G.A., Ferreira, L., Yacu, G., 2015. Geologic evolution of the Iraqi Zagros
556 and its influence on the distribution of hydrocarbons in the Kurdistan region. AAPG Bulletin,
557 V.99, No.2, 231-272, DOI: 10.1306/06271413205.

558 Feng, H., Bancroft, J.C., 2006. AVO principles, processing and inversion. CREWES Research
559 Report, Vol. 18, 1-19.

560 Fink, P., Schuh, M., Ahmad, N., Koehazy, R., 2004. Can the American Securities and Exchange
561 Commission and the central limit theorem ever become friends? A practical proposal for
562 reconciliation from OMV's Sawan Reserves Estimation exercise. PAPG/SPE Annual Technical
563 Conference, 8-9 October, Islamabad, Pakistan.

564 Floridia, C., Teles, N.T., 1998. Effects of anisotropy in the AVO analysis. SEG Technical
565 Program, Expanded Abstracts, 212-215. doi:10.1190/1.1820378.

566 Gassmann, F., 1951. Über die Elastizität poröser Medien.Viertel.Naturforsch.Ges. Zürich, 96, 1-
567 23.

568 Goodway, B., Perez, M., Varsek, J., Abaco, C., 2010. Seismic petrophysics and isotropic-
569 anisotropic AVO methods for unconventional gas exploration. The Leading Edge, 29(12), 1500-
570 1508. Doi: 10.1190/1.3525367.

571 Graebner, M., 1992. Plane-wave reflection and transmission coefficients for a transversely
572 isotropic solid. Geophysics, 57(11), 1512-1519, doi:10.1190/1.1443219.

573 Grechka, V.,1998. AVO analysis in finely layered azimuthally anisotropic media. SEG Technical
574 Program, Expanded Abstracts. 1649-1652. doi: 10.1190/1.1820238.

575 Iqbal, M.W.A., Shah, S.M.I., 1980. A guide to the stratigraphy of Pakistan, Geological Survey
576 of Pakistan, Records. Geol. Surv. Pak. Quetta, 53-34.

577 Jakobsen, M., Johansen, T.A., 1999. A test of ANNIE based on ultrasonic measurements on a
578 shale. J. Seis. Explor.issue No. 8, 77-89.

579 Jakobsen, M., Hudson, J.A., Johansen, T.A., 2003a. T-matrix approach to shale acoustics.
580 Geophysical Journal International, Issue No.154, 533-558.

581 Jakobsen, M., Johansen, T.A., 2000. Anisotropic approximations for mud rocks: A seismic
582 laboratory study. Geophys. **65,** 1711-1725.

583 Jakobsen, M., Johansen, T.A., McCann, C., 2003b. The acoustic signature of fluid flow in
584 complex porous media. Journal of Applied Geophysics, 54, 219-246.

585 Jinhu, D., He, L., Desheng. M., Jinhua, F., Yuhua, W., Zhou, T., 2014.Discussion on effective
586 development techniques for continental tight oil in China. Petroleum Exploration and
587 Development, Volume 41, Issue 2, 217-224.

588 Kadri, I.B., 1995. Petroleum geology of Pakistan: Pakistan Petroleum Limited. Graphic
589 Publishers Karachi.

590 Katz, B., Lin, F., 2014. Lacustrine Basin unconventional Resource Plays: Key differences.
591 Marine and Petroleum Geology, Volume 56, 255-265.

592 Kim, K.Y., Wrolstad, K.H., Aminzadeh, F., 1993. Effects of Transverse Isotropy on P-wave
593 AVO for gas sands. Geophysics, 58, 883-888.

594 Krois P, Mahmood T, Milan, G., 1998. Miano field, Pakistan a case history of model driven
595 exploration. Proceedings of the Pakistan Petroleum Convention, Pakistan Association of
596 Petroleum Geologists Islamabad, 111-131.

597 Kumar, D., Hoversten, G.M., 2012. Geophysical model response in a shale gas. 9th Biennial
598 international conference & Exposition on Petroleum Geophysics, Hyderabad, India.

599 Kurniawan, F., 2005. Shaly Sand Interpretation Using CEC-Dependent Petrophysical
600 Parameters, MS Dissertation, Louisiana State University and Agricultural and Mechanical
601 College.

602 Leaney, W.S., 1993. AVO and anisotropy from logs and walkaways. Exploration Geophysics,
603 24, 623-630.

604 Li, V., Tsvankin, I., Alkhalifah, T., 2016. Analysis of RTM extended images for VTI media
605 Geophysics, Vol. 81, NO.3, S139–S150, DOI: 10.1190/GEO2015-0384.1.

606 Luo, X., Lin, Y., Wu, L., Yao, F., 2005. Estimation of anisotropy parameters in VTI Media from
607 surface P-wave seismic data and VSP in Tarim Basin, China. SEG Annual Meeting, Houston.
608 178-181.

609 Margesson, R.W., Sondergeld, C.H., 1999. Anisotropy and amplitude versus offset: a case
610 history from the West of Shetlands. Proceedings of the 5th Conference, 635-643. Petroleum
611 Geology '86 Ltd. Published by the Geological Society, London.

612 Mavko, G., Mukerji, T., Dvorkin, J. 2009. The Rock Physics Handbook: Tools for Seismic
613 Analysis in Porous Media. Cambridge University Press, UK.

McGlade, C., Speirs, J., Sorrell, S., 2012. A review of regional and global estimates of unconventional gas resources. A report to the Energy Security Unit of the Joint Research Centre of the European Commission.

McPhee, C.A., Enzendorfer, C.K., 2004. Sand management solutions for high-rate gas wells, Sawan field. SPE, Sindh.

Munir, K., Iqbal, M.A., Farid, A., Shabih, S.M. 2011. Mapping the productive sands of Lower Goru Formation by using seismic stratigraphy and rock physical studies in Sawan area, southern Pakistan: a case study. Journal of Petroleum Exploration & Production Technology, issue No.1, 33-42, doi:10.1007/s13202-011-0003-9.

Nourollah, H., Urosevic M., Keetley, J., 2015. Seal potential of shale sequences through seismic anisotropy: Case study from Exmouth Sub-basin, Australia. Society of Exploration Geophysicists Vol. 3, Issue No. 4, T257-T267.

Pujol, J., 2003. Elastic Wave Propagation and Generation in Seismology. ISBN 0-521-52046-0, Cambridge University Press, UK, 160-161.

Quadri, V.N., Shuaib, M.,1986. Hydrocarbon prospects of Southern Indus Basin, AAPG Bulletin, v. 70, pp.730–747.

Rodriguez, K., Hodgson, N., Hewitt, A., 2016. The future of oil exploration. First Break, Vol 34, issue No 2, 95-101.

Rüger, A., 2002. Reflection Coefficients and Azimuthal AVO Analysis in Anisotropic Media: Geophysical Monograph Series, No. 10, Society of Exploration Geophysics.

Rüger, A.,1998. Variation of P-wave reflectivity with offset and azimuth in anisotropic media. Geophysics, issue Nno.63, 935-947.

636 Sams, M.S., Andrea, M., 2001. The effect of clay distribution on the elastic properties of
637 sandstones. Geophysical Prospecting, 49,128-150.

638 Saxena, K., Tyagi, A., Klimentos, T., Morriss, C., Mathew, A. 2006. Evaluating Deepwater Thin-
639 Bedded Reservoirs with the RT Scanner. Petromin, Kaula Lumpur.

640 Sayers, C.M. 2013. Rock Physics for Reservoir Exploration, Characterisation and Monitoring.
641 Geophysical Prospecting, 61, 251–253. doi: 10.1111/1365-2478.12034.

642 Sayers, C.M., 1998. Long-wave seismic anisotropy of heterogeneous reservoirs, Geophysical J.
643 Int. 132, 667-673.

644 Sayers, C.M., Rickett, J.E., 1997. Azimuthal variation in AVO response for fractured gas sands,
645 Geophysical Prospecting, 45, 165-182.

646 Shahraini, A., Ali, A., Jakobsen, M. 2011. Seismic history matching in fractured reservoirs using
647 a consistent stiffness-permeability model: Focus on the effects of fracture aperture, Geophysical
648 Prospecting, 59, 492-505.

649 Sone, H., Zoback, M.D., 2013. Mechanical properties of shale-gas reservoir rocks Part 2: Ductile
650 creep, brittle strength, and their relation to the elastic modulus. Geophysics , Vol. 78, No. 5,
651 D393-D402.

652 Tarantola, A., 2005. Inverse Problem Theory and Methods for Model Parameter Estimation.
653 Society for Industrial and Applied Mathematics, USA.

654 Thomas, E.C., Stieber S.J., 1975. The distribution of shale in sandstones and its effect on
655 porosity. SPWLA 16th Annual Logging Symp., 4-7 June1975.

656 Thomsen, L., 1995. Elasticity anisotropy due to aligned cracks in porous rock, Geophysical
657 Prospecting, 43, 805-829.

658 Thomsen, L.,1986. Weak elastic anisotropy. Geophysics,51(10), 1954-1966.

659 Tsvankin, I., 1997a. Anisotropic parameters and P-wave velocity for orthorhombic media
660 Geophysics, 62, 1292–1309.

661 Tsvankin, I., 1997b. Reflection move out and parameter estimation for horizontal transverse
662 isotropy. Geophysics, issue No.62, 614-629.

663 Tyagi, A.K., Guha, R., Voleti, D., Saxena, K., 2009. Challenges in The Reservoir
664 Characterization of a Laminated Sand Shale Sequence. 2nd SPWLA-India Symposium,
665 November 19-20.

666 Uden, R., Dvorkin, J., Walls, J., Carr, M., 2004. Lithology substitution in a sand/shale sequence.
667 ASEG 17th Geophysical Conference and Exhibition, Sydney.

668 Wandrey, C.J., Law, B.E., Shah, H.A., 2004. Sembar Goru/Ghazij composite total petroleum
669 system Indus and Sulaiman-Kirthar geologic Provinces Pakistan and India. US Geological
670 Survey, USA; Geological Survey Bulletin.

671 Wang, L., Dai, H., Li, X.Y., 2006. Estimating anisotropic parameters from PS converted-wave
672 data: a case study. British Geological Survey, Xianyi Sun, Petro China, Daqing Oil Field.

673 Wang, Y., 2011. Seismic anisotropy estimated from P-wave arrival times in cross hole
674 measurements. Geophysical Journal International, 184, 1311-1316.

675 Wood, A.W., 1955. A Textbook of Sounds, New York, McMillan Co. USA.

676 Wright, J., 1987. The effects of transverse isotropy on reflection amplitude versus offset.
677 Geophysics, 52, 564-567.

678 Xu, S., Wu, X., Huang, X., Yin, H., 2005. Evaluation of Anisotropic Rock Properties in
679 Sedimentary Rocks from well log. Offshore Technology Conference Houston, TX, USA.

680 Zaigham, N.A., Mallick, K.A., 2000. Prospect of hydrocarbon associated with fossil-rift
681 structures of the southern Indus basin, Pakistan. AAPG, Bull 84(11), 1833-1848.

682 Zhang, H., Brown, R.J., 2001. A review of AVO analysis, CREWES Research Report, Volume
683 13, 337-378

684 Zhu, Y., Xu, S., Payne, M., Martinez, A., Liu, E., Harris, C., Bandyopadhyay, K., 2012.
685 Improved Rock-Physics Model for Shale Gas Reservoirs. SEG Technical Program Expanded
686 Abstracts, 1-5.doi: 10.1190/segam2012-0927.1

687 Zoeppritz, K.E., 1919. On the reflection and propagation of seismic waves. Göttinger
688 Nachrichten, 1(5), 66-84.

689

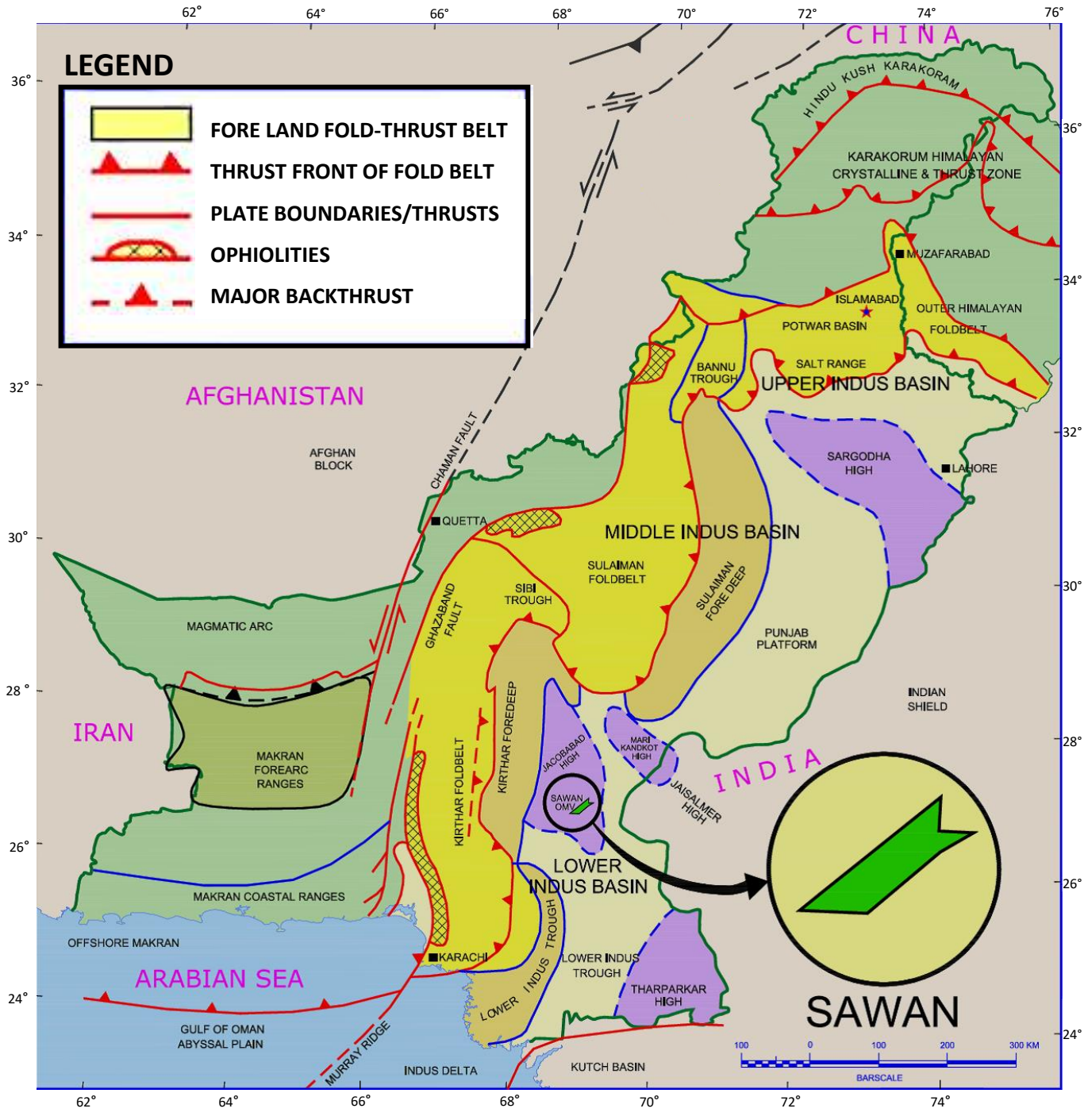

690

691 Figure 1a: Regional map showing the regional structural setting of Pakistan and the location of

692 multiple sedimentary basins in this country. The location of Sawan gas field is highlighted by

693 the black circle.

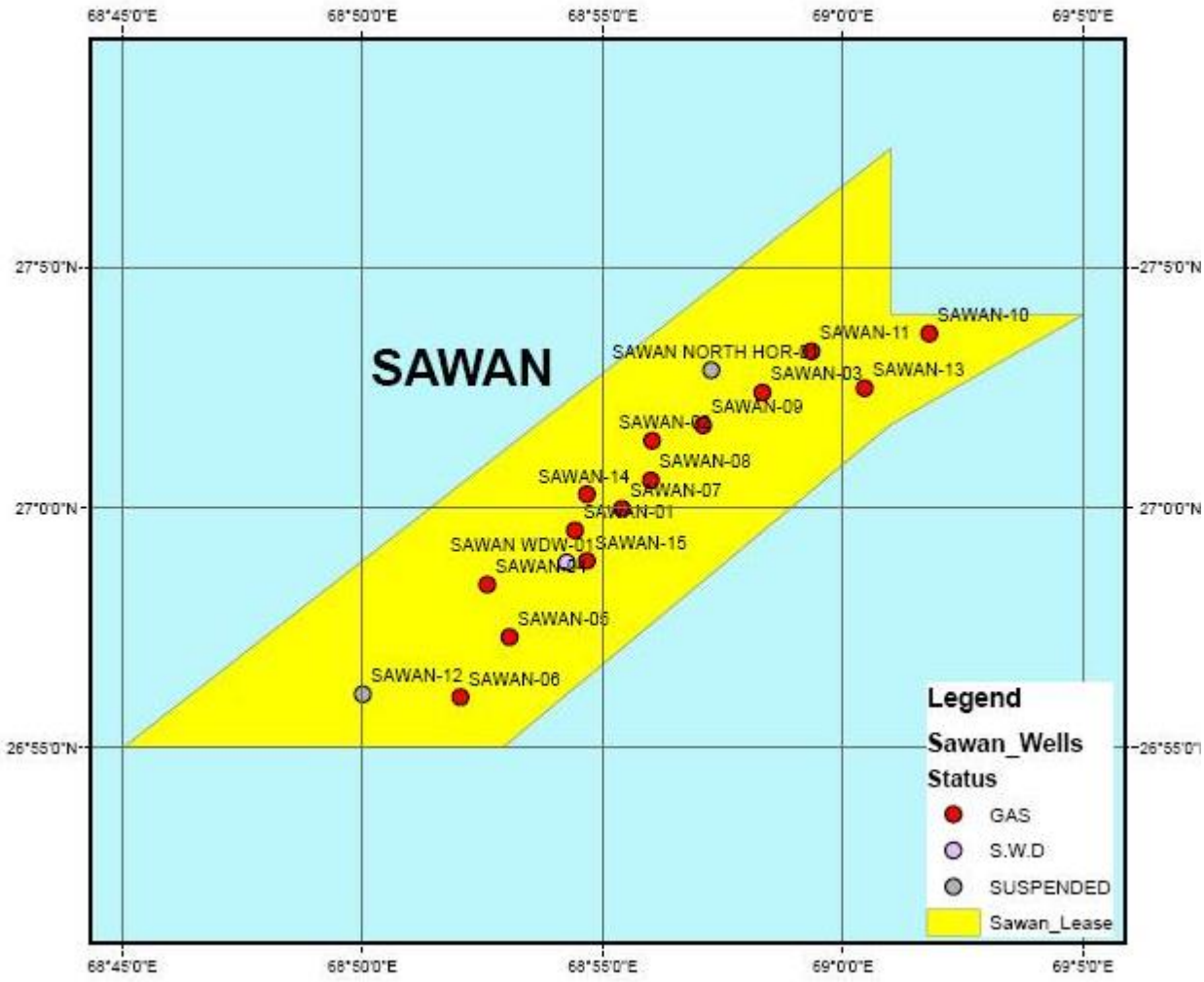

694

695 Figure-1b: Local map showing the boundaries of the Sawan gas field and the relative location

696 of exploration wells in the study area.

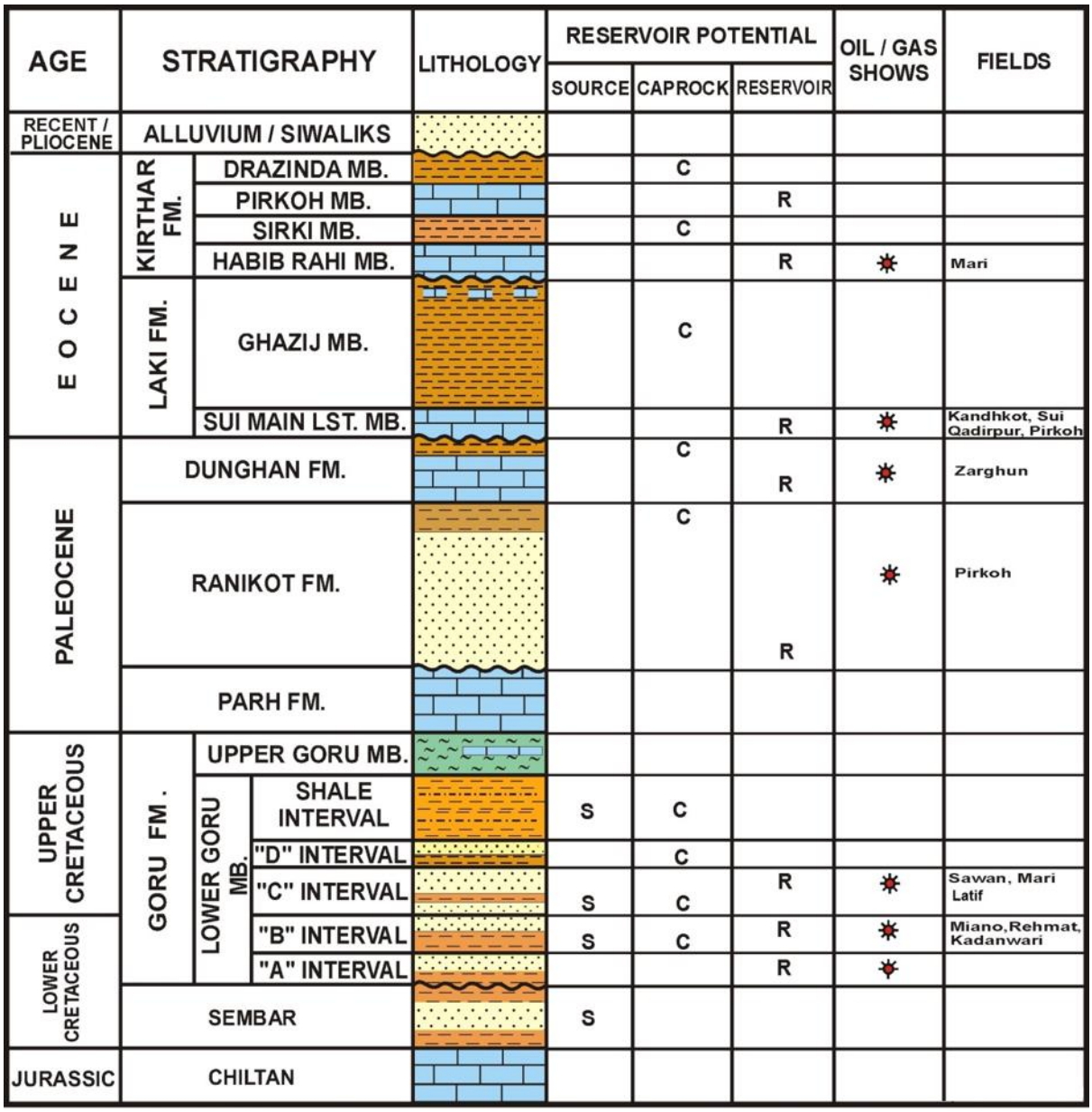

Figure 2: Generalised stratigraphy of the Sawan gas field highlighting the presence of multiple lithological units, including the Lower Goru C-sand interval and shaley intervals within and adjacent to these reservoir sands. This C-sand interval comprises the principal gas-producing reservoir of the Sawan field (Azeem et al., 2015).

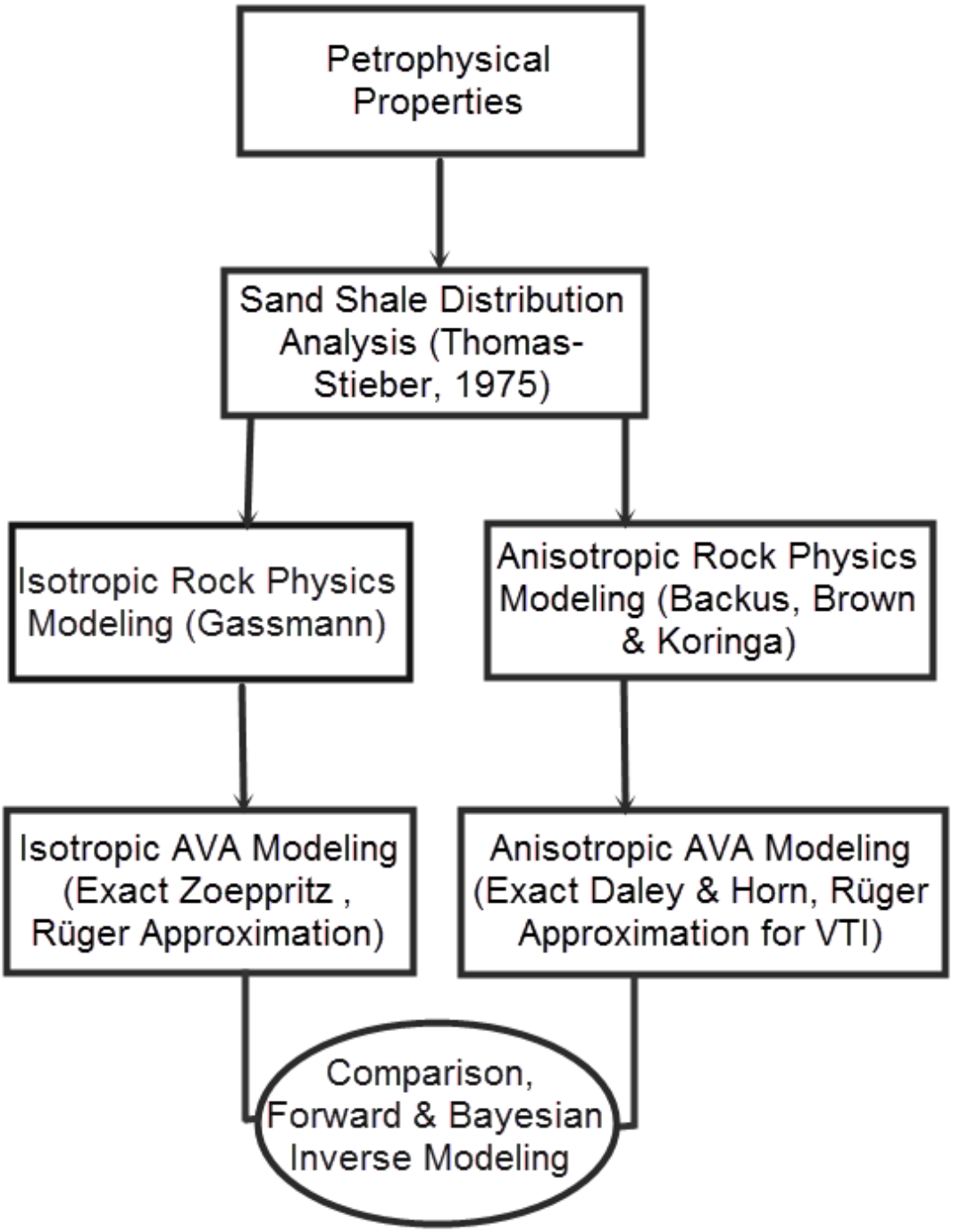

703
704 Figure 3: Work Flow diagram showing the methodology adopted to compare isotropic and
705 anisotropic AVA modelling.
706

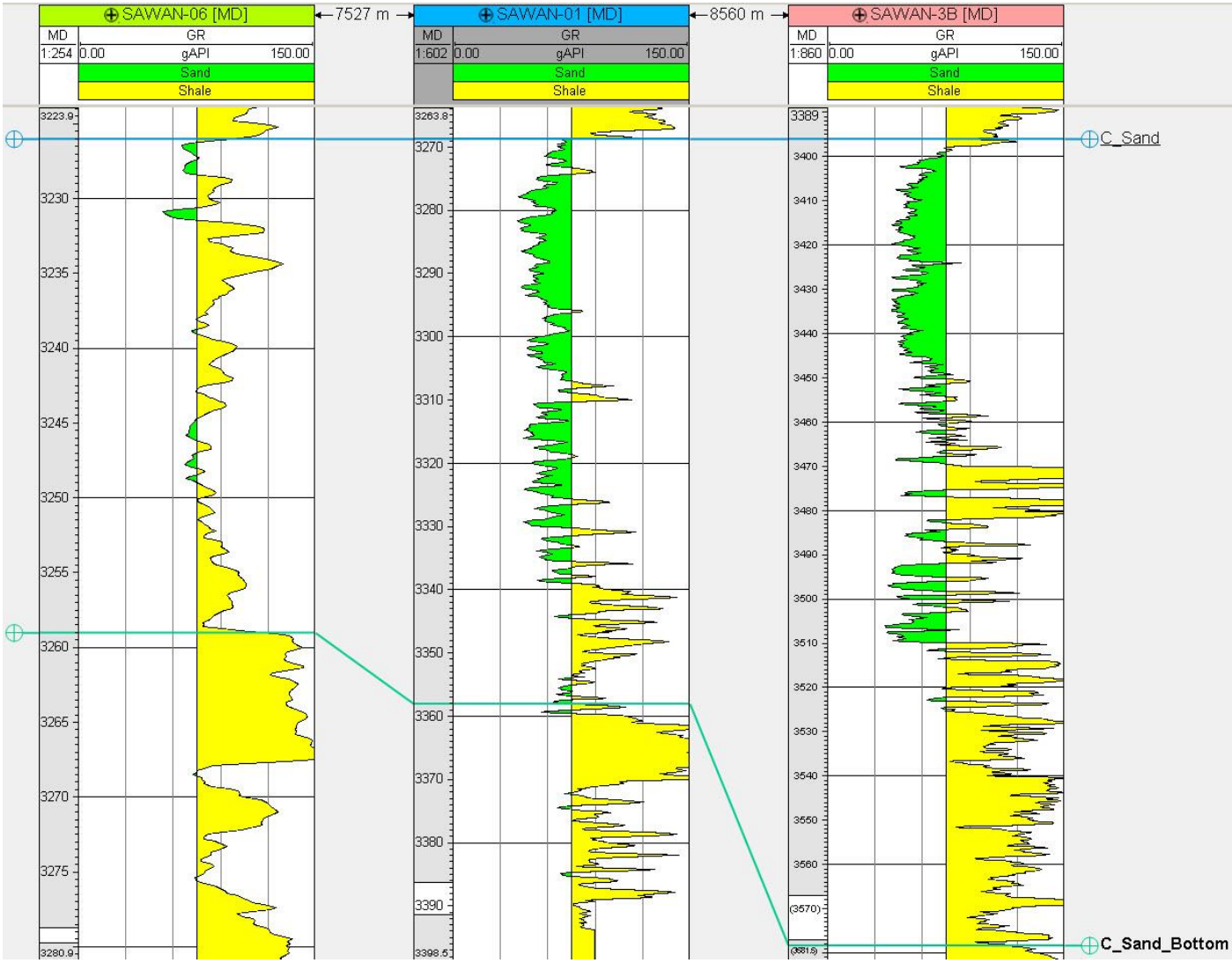

707

708 Figure 4 Well-log correlations for the Lower Goru C-sand and shale intervals in the three exploration wells used in AVA modelling.

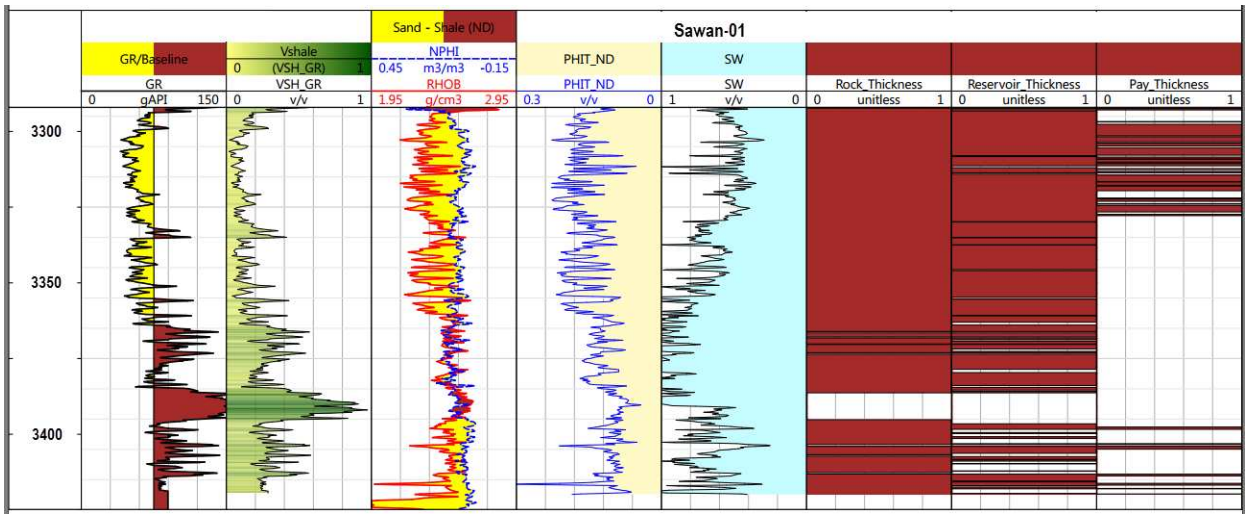

709

710 Figure 5: Results of petrophysical analyses for the estimation of reservoir properties of sand-

711 shale intervals in the Sawan-01 well.

712

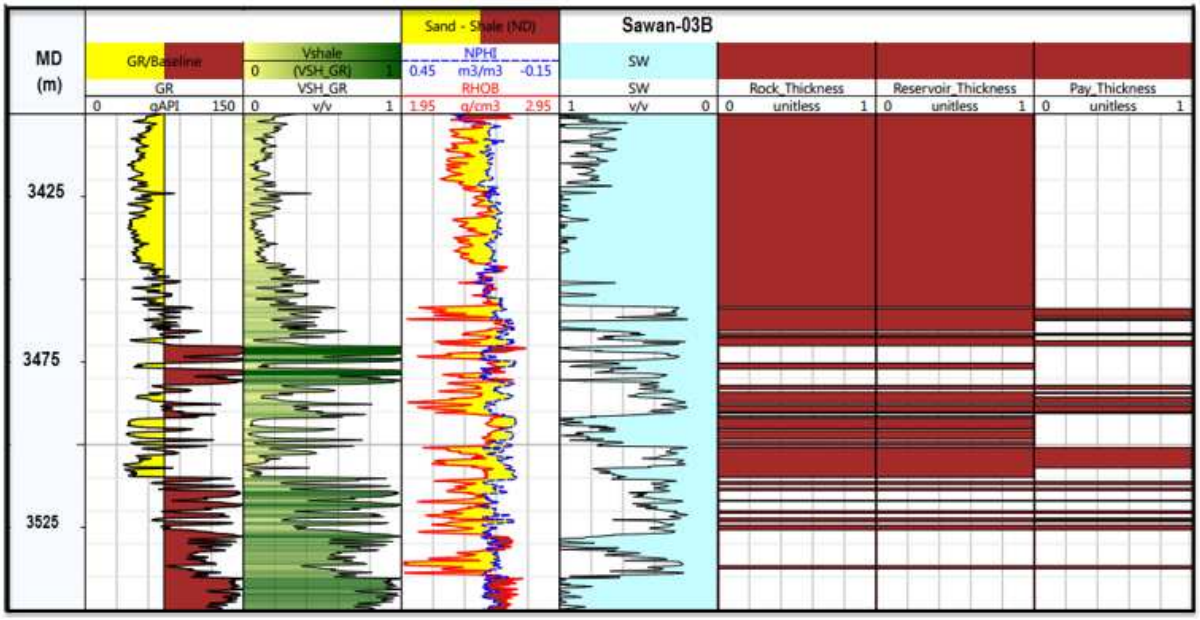

Figure 6: Results of petrophysical analyses for the estimation of reservoir properties of sand-shale intervals in the Sawan-3B well.

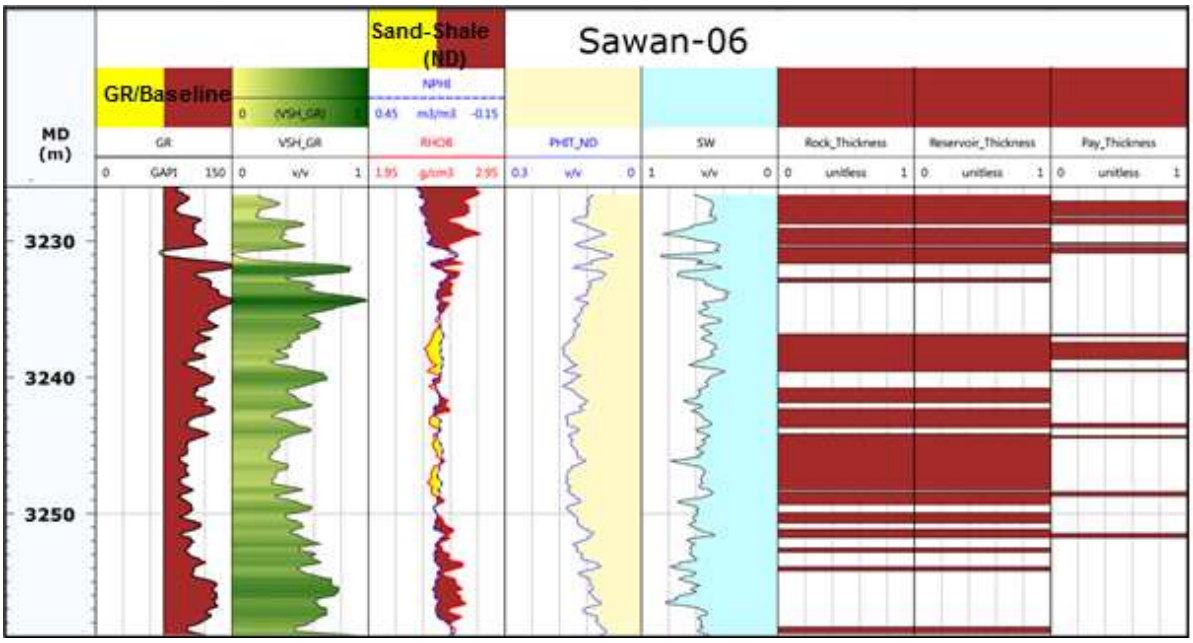

716

717 Figure 7. Results of petrophysical analyses for the estimation of reservoir properties of sand-

718 shale intervals in the Sawan-06 well.

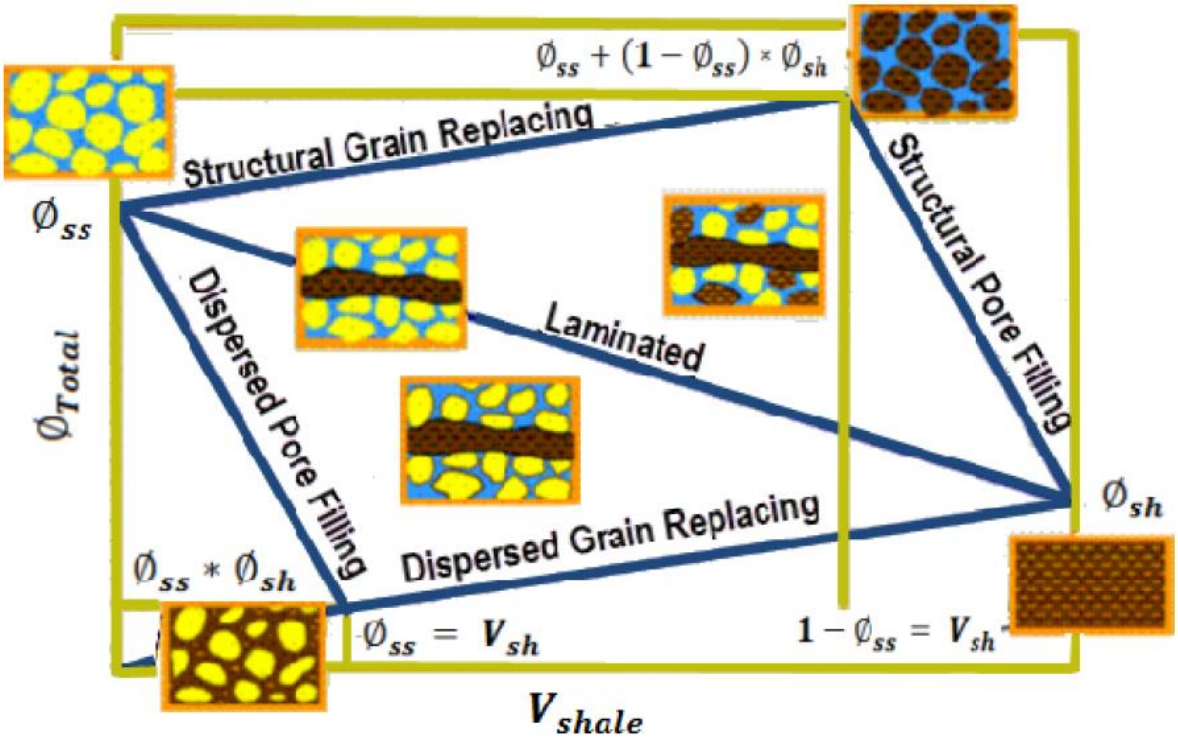

719

720 Figure 8: Shale distribution model proposed by Thomas and Strieber (1975) (figure modified
721 from Tyagi et al., 2009). In this diagram, V_{shale} is the volume of shale, ϕ_{total} is the total
722 porosity, ϕ_{max} is the maximum porosity, and ϕ_{sh} is the porosity in shales.

723

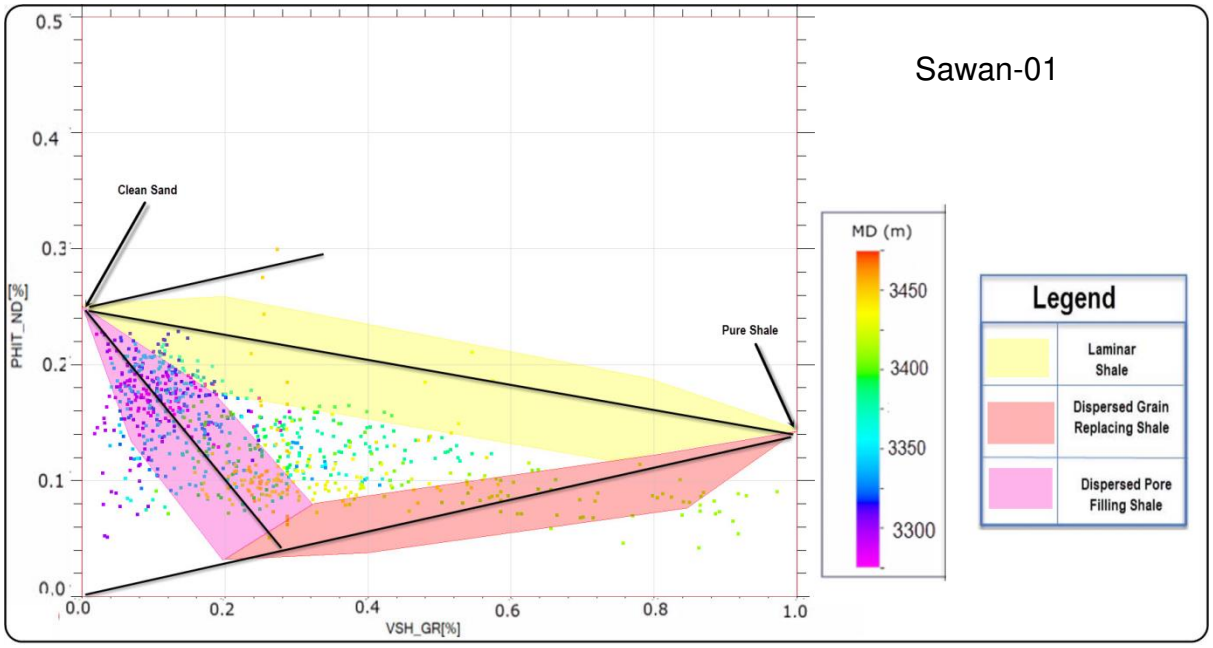

Figure 9: Cross-plots between volume of shale (X-axis) and total porosity (Y-axis). Based upon the position of data points, shale distribution was characterised within the C-sand reservoir in the Sawan-01 well.

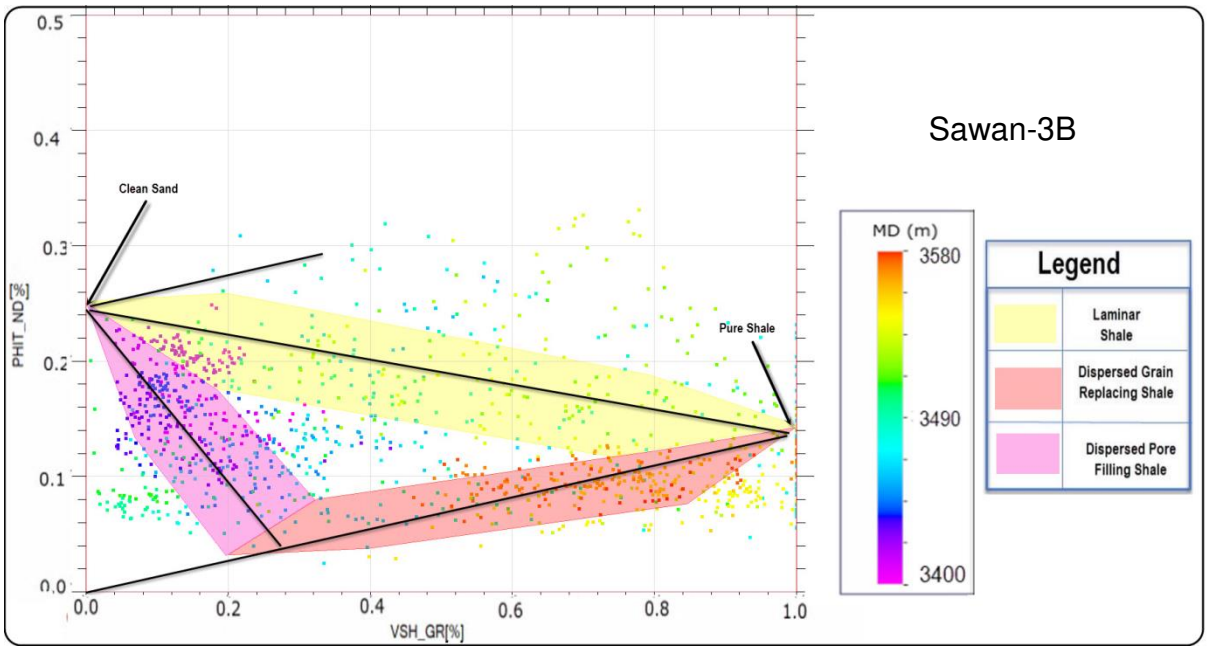

730

731 Figure 10: Cross-plots between volume of shale (X-axis) and total porosity (Y-axis). Based
732 upon the position of data points, shale distribution was characterised within the C-sand
733 reservoir in the Sawan-3B well.

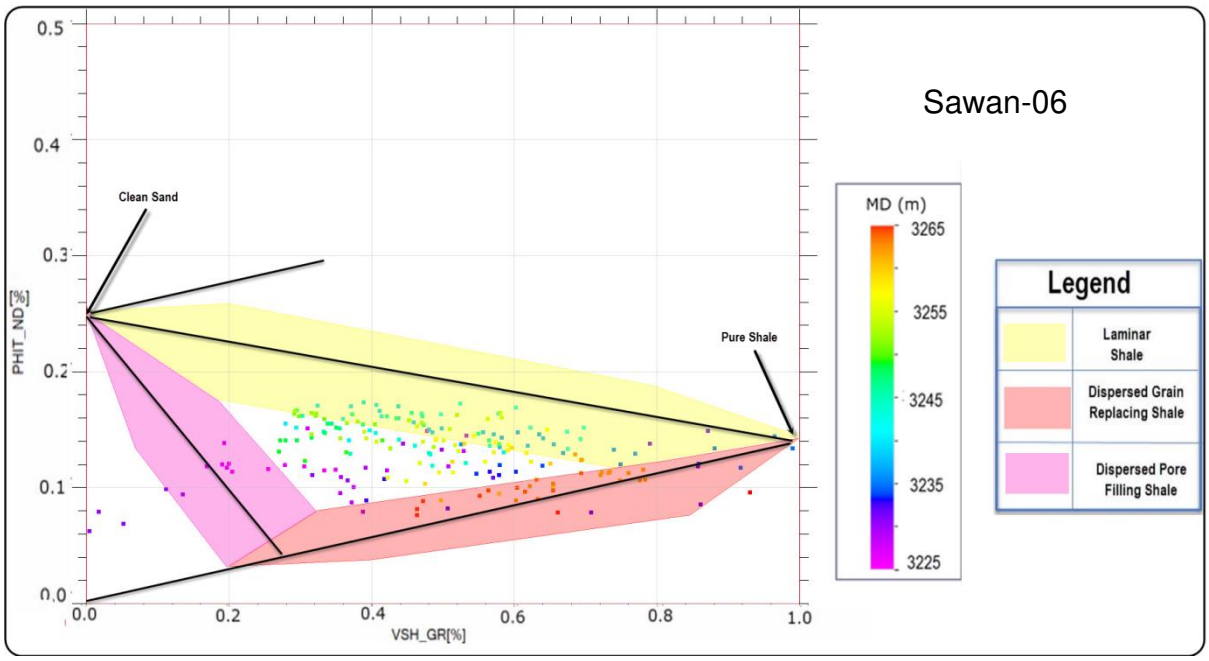

734

735 Figure 11: Cross-plots between volume of shale (X-axis) and total porosity (Y-axis). Based
736 upon the position of data points, shale distribution was characterised within the C-sand
737 reservoir in the Sawan-06 well.

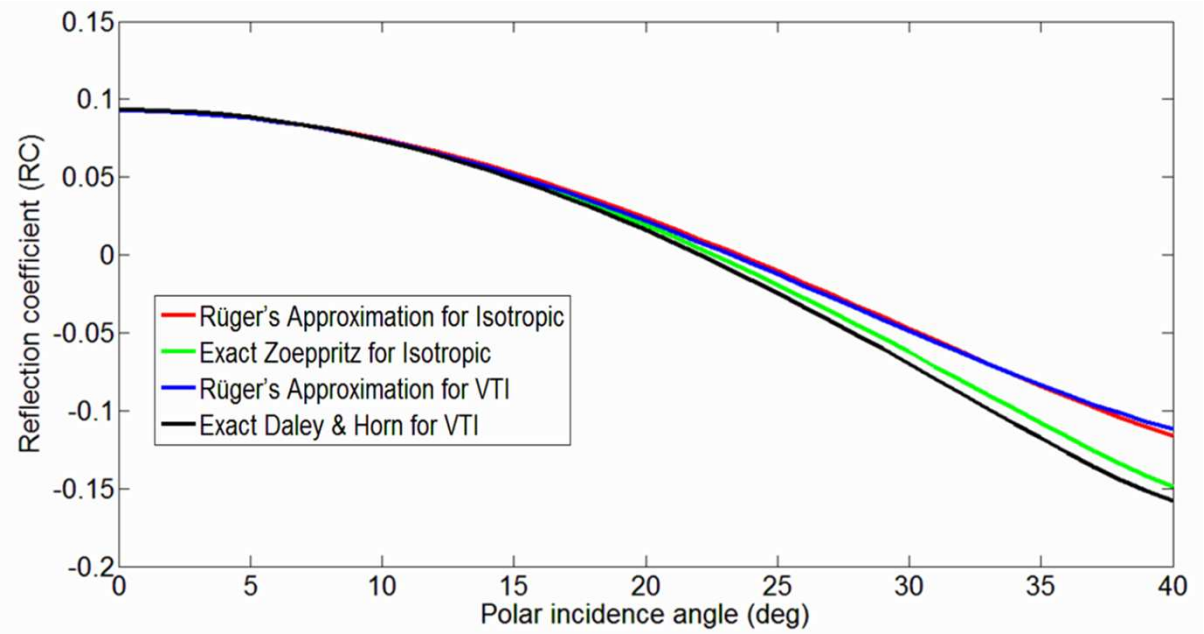

738

739 Figure 12: Angle-dependent reflection coefficient data generated through the exact and

740 approximate solutions of PP-wave for isotropic and anisotropic (VTI) media at the top of C-

741 sand reservoir (Sawan-01 well).

742

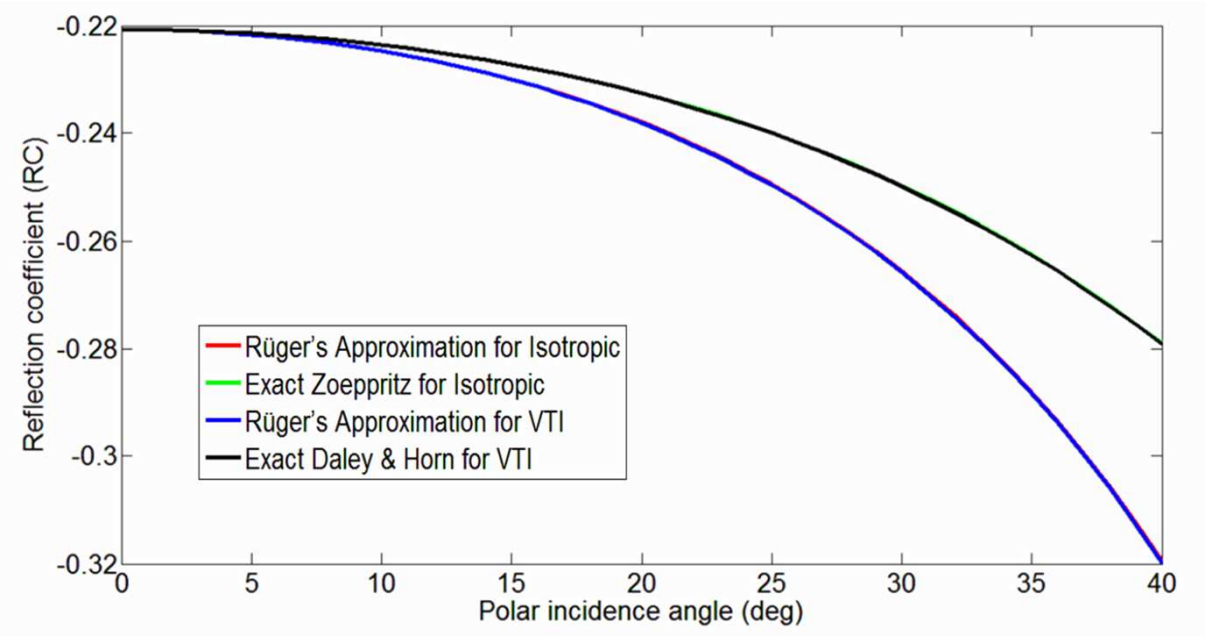

743

744 Figure 13: Angle-dependent reflection coefficient data generated through the exact and

745 approximate solutions of PP-wave for isotropic and anisotropic (VTI) media at the top of C-

746 sand reservoir (Sawan-3B well).

747

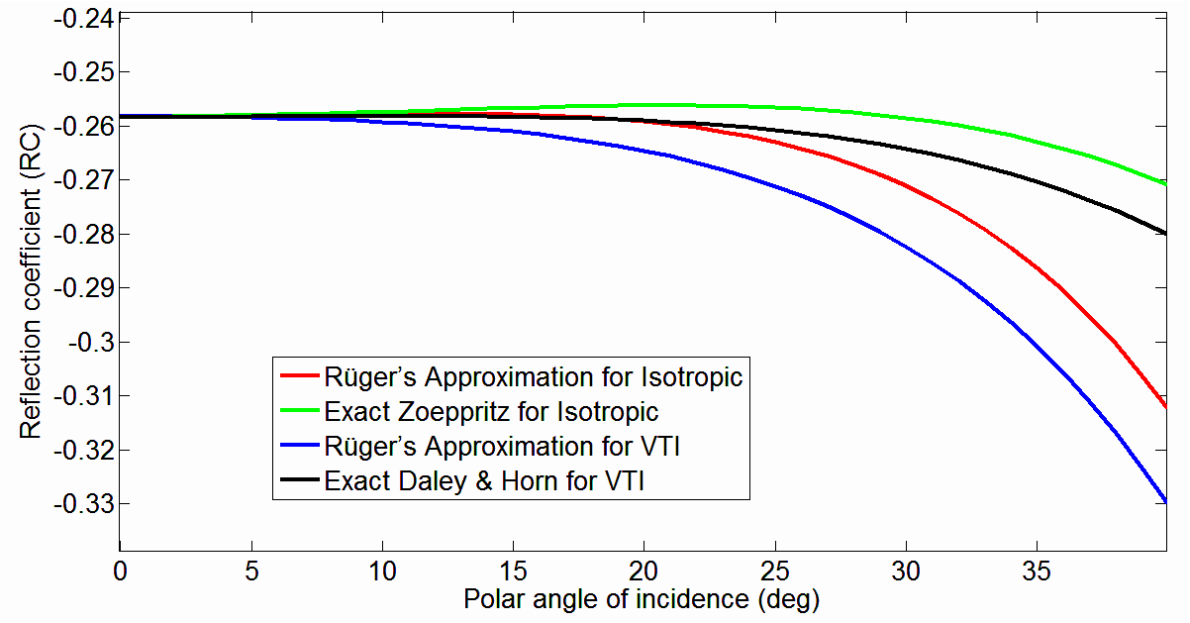

748

749 Figure 14: Angle-dependent reflection coefficient data generated through the exact and

750 approximate solutions of PP-wave for isotropic and anisotropic (VTI) media at the top of C-

751 sand reservoir (Sawan-06 well).

752

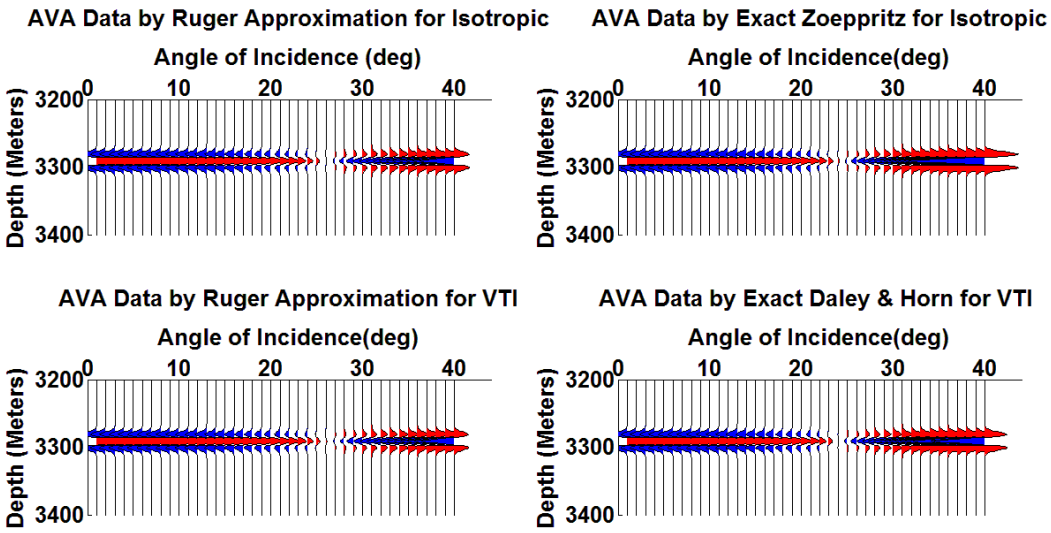

753

754 Figure 15: Seismic AVA response for the Lower Goru C-sand, Sawan-01 well.

755

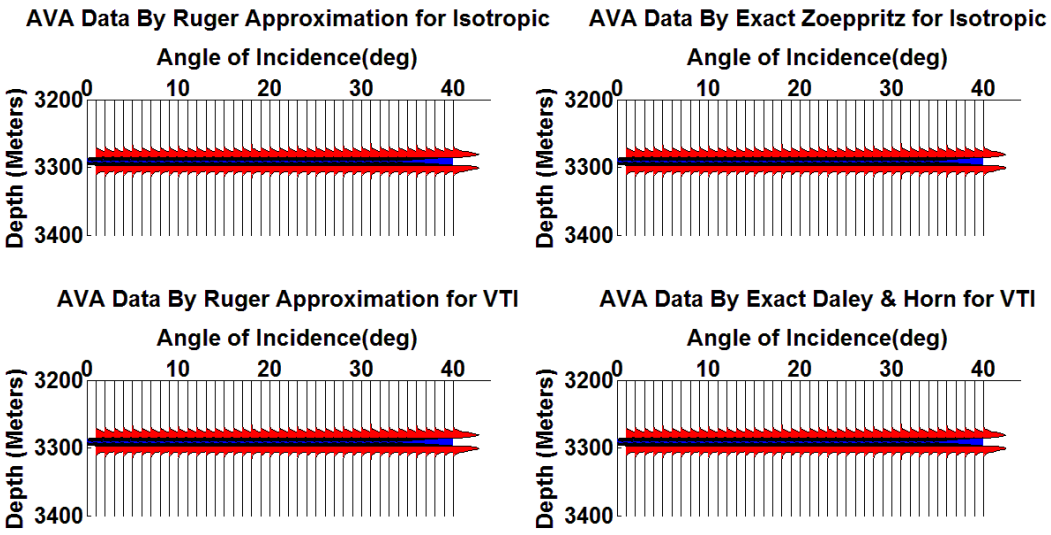

Figure 16: Seismic AVA response for the Lower Goru C-sand, Sawan-3B well.

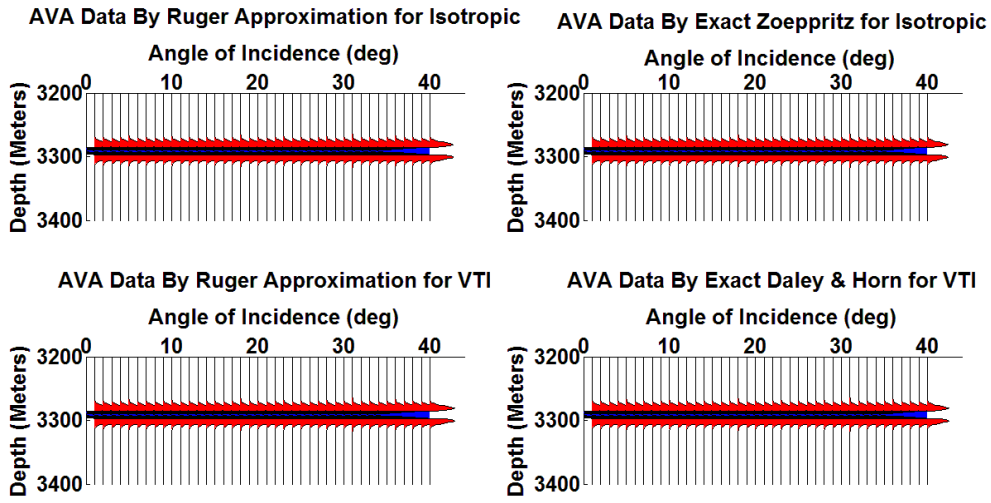

759

760 Figure 17: Seismic AVA response for the Lower Goru C-sand, Sawan-06 well.

761

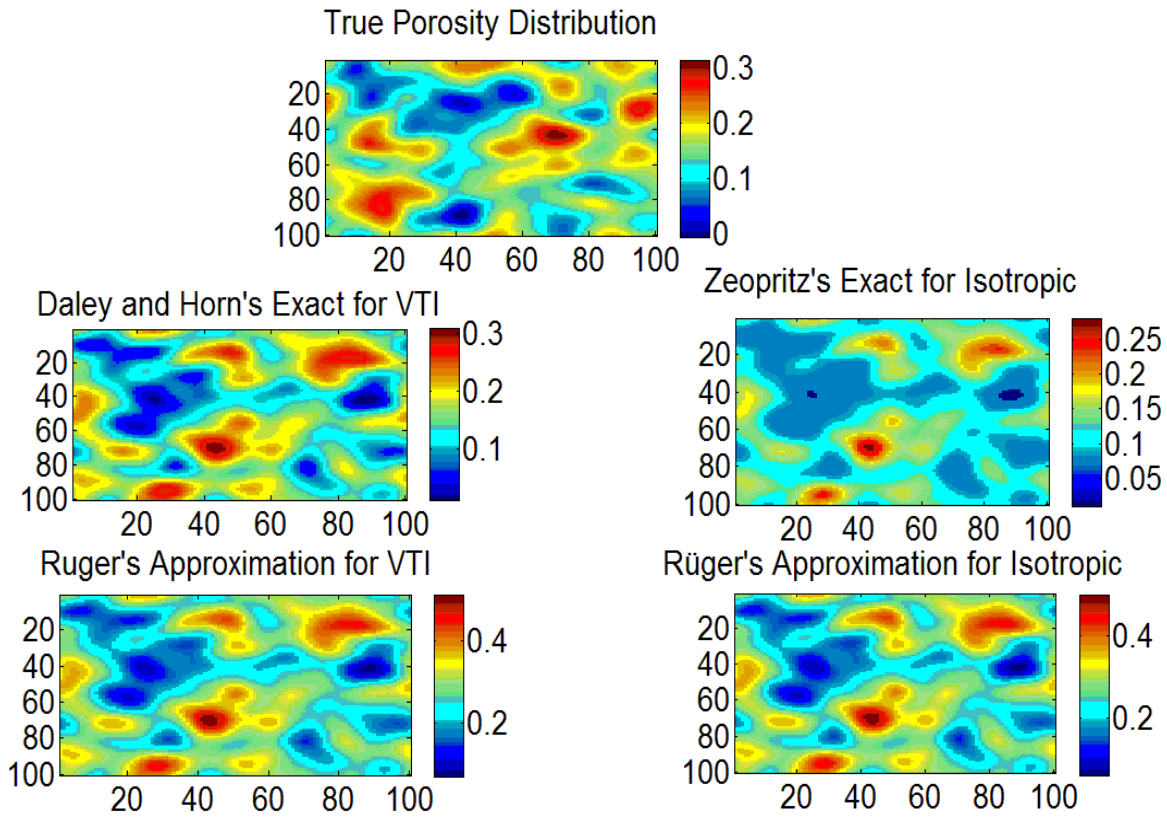

762

763 Figure 18: Maps highlighting the inversion with 20% uncertainty for true porosity distribution
764 (top) generated via a correlated Gaussian field distribution throughout the reservoir interval at
765 100×100 grid blocks. These porosity plots were compiled via maximum a posteriori solution
766 under Bayesian settings utilising the rock physical properties of C-sand reservoir interval
767 (3268-3432 m) with exact and approximate solutions of PP-reflection coefficients for the
768 isotropic and anisotropic (VTI) cases. Inversion results show that Daley & Horn's (1977) exact
769 solution for VTI (left in 2nd row) returns porosity trends that are accurately aligned with the
770 true porosity distribution of the reservoir.

771

Reservoir Properties	**Sawan-01**	**Sawan-3B**	**Sawan-06**
Depth Range (m)	3268-3432	3398-3592	3227-3312
Gross Thickness (m)	164	184	85
Net Reservoir Thickness (m)	80	126	36
Net Pay Thickness (m)	24	58	20
Avg Porosity (%)	15	14	12
Avg Volume of Shale (%)	28	22	34
Average Water Saturation (%)	46	40	45

772 **Table 1**: Reservoir properties of the Sawan wells used in this study.

773

Cut-off	GR<=75 API	0.1<=NPHI<=0.45	Sw<=50%
Rock Thickness (m)	Yes	No	No
Net Reservoir Thickness (m)	Yes	Yes	No
Net Pay Thickness (m)	Yes	Yes	Yes

774 **Table 2**: Details of cut-off values used in the calculation of reservoir properties in Table 1.

775

Well	Formation	$V_p(\alpha)$	$V_s(\beta)$	Density(ρ)	Porosity(ϕ)
Sawan-01	Sand	4165	4112	2.32	0.15
	Shale	2668	2170	2.67	0.08
	Overburden	2874.5	2367.5	2.54	
Sawan-3B	Sand	4251	2562	2.44	0.13
	Shale	4487	2628	2.60	0.10
	Overburden	4258	2547	2.62	
Sawan-06	Sand	4148.628	2579.0	2.51	0.13%
	Shale	4462.847	1741.0	2.61	0.085%
	Overburden	4322.960	2520.0	2.57	

776 **Table 3**: Mechanical properties of reservoir sand, intra-reservoir shale layers and overburden
777 used in the calculation of reflection coefficients.
778

Material	**Shear modulus (GPa)**	**Bulk modulus (GPa)**	**Density (g/cm^3)**
Solid Mineral (Quartz)	44	37	2.65
Gas	0.0	0.025	0.065
Fluid (water/brine)	0.0	2.2	1.035

Table 4: Values of elastic moduli and densities for solid mineral and fluid used in our rock physics modelling.

779

Appendix-A

Backus Averaging Approach

The effective stiffness is anisotropic for a stratified medium composed of transversely isotropic layers in the limit of long-wavelength, and represented by the Backus (1962) matrix below (Mavko et al., 2009):

$$\begin{bmatrix} A & B & F & 0 & 0 & 0 \\ B & A & F & 0 & 0 & 0 \\ F & F & C & 0 & 0 & 0 \\ 0 & 0 & 0 & D & 0 & 0 \\ 0 & 0 & 0 & 0 & D & 0 \\ 0 & 0 & 0 & 0 & 0 & M \end{bmatrix}, \qquad M = \frac{1}{2}(A - B), \tag{A-I}$$

where A, B, C, D and F are the five independent elastic constants [i.e., $C_{11}, C_{13}, C_{33}, C_{55}\&C_{66}$]. In terms of P- and S-wave velocities (V_P and V_S) and densities (ρ), the five independent elastic constants can be written as:

$$A = \left\langle 4\rho V_S^2 \left[1 - \frac{V_S^2}{V_P^2}\right] \right\rangle + \left\langle 1 - 2\frac{V_S^2}{V_P^2} \right\rangle^2 \left\langle \left(\rho V_P^2\right)^{-1} \right\rangle^{-1}, \tag{A-II}$$

$$B = \left\langle 2\rho V_S^2 \left[1 - \frac{2V_S^2}{V_P^2}\right] \right\rangle + \left\langle 1 - 2\frac{V_S^2}{V_P^2} \right\rangle^2 \left\langle \left(\rho V_P^2\right)^{-1} \right\rangle^{-1}, \tag{A-III}$$

$$C = \left\langle \left(\rho V_P^2\right)^{-1} \right\rangle^{-1}, \tag{A-IV}$$

$$D = \left\langle \left(\rho V_S^2\right)^{-1} \right\rangle^{-1}, \tag{A-V}$$

$$F = \left\langle 1 - 2\frac{V_S^2}{V_P^2} \right\rangle^2 \left\langle \left(\rho V_P^2\right)^{-1} \right\rangle^{-1}, \tag{A-VI}$$

794 $$M = \left\langle \rho V_S^{\,2} \right\rangle. \qquad \text{(A-VII)}$$

795 The brackets $\langle \cdot \rangle$ indicate averages of the enclosed properties weighted by their volumetric
796 proportions. Once the five independent constants are obtained, the Thomsen anisotropy
797 parameters for VTI can be obtained using the relationships given by Thomsen (1986, 1995):

798 $$\gamma = \frac{M-D}{2D}, \qquad \text{(A-VII)}$$

799 $$\varepsilon = \frac{A-C}{2C}, \qquad \text{(A-VIII)}$$

800 $$\delta = \frac{(F+D)^2-(C-D)^2}{2C(C-D)}. \qquad \text{(A-IX)}$$

801 In order to calculate the effect of fluid saturation on the effective properties of a sand-shale
802 layered medium, we have used the Gassmann (1951) equation for isotropic media, and the
803 relationships of Brown and Korringa (1975) for anisotropic (VTI) media (Ali et al., 2011;
804 Shahraini et al., 2011).

805

Appendix-B

1. Gassmann (1951) fluid substitution model for isotropic media

As the dry composite sand-shale medium was assumed as isotropic in this work, we used the low frequency Gassmann (1951) model (Equation B-I) applicable to well-connected porous media under isobaric conditions. We used this latter model in order to incorporate fluid effects into the effective mechanical properties calculated in our own models. Equation (B-I) defines a relationship between saturated bulk modulus, bulk modulus of the skeleton of the rock, bulk modulus of mineral comprising rock matrix, fluid bulk modulus and porosity. A typical form of the Gassmann (1951) equation is as follows:

$$K_{sat} = K_{dry} + \left\{ \frac{\left(1-\left({K_{dry}}/{K_{grian}}\right)\right)}{\left(\frac{\phi}{K_{fluid}}+\frac{1-\phi}{K_{grian}}-\frac{K_{dry}}{K_{grian}^2}\right)} \right\}. \qquad \text{(B-I)}$$

Here 'K_{sat}' is the saturated rock bulk modulus, 'K_{dry}' is the frame or dry bulk modulus, 'K_{grian}' is the grain bulk modulus, 'K_{fluid}' corresponds to the fluid bulk moduli, and 'ϕ' is the porosity.

2. Brown and Korringa (1975) relations for fluid effects of an anisotropic medium (VTI)

In order to calculate the effect of fluid saturation on the effective properties of a sand-shale interval, assuming it as VTI medium, we have used the anisotropic relations of Brown and Korringa (1975), which can be written in the symbolic or matrix notation as (Ali et al., 2011):

$$\mathbf{S}^{*} = \mathbf{S}_{\mathbf{d}}^{*} + \frac{\left((\mathbf{S}_{\mathbf{d}}^{*} - \mathbf{S}_{\mathbf{m}}) : (\mathbf{I}_2 \otimes \mathbf{I}_2) : (\mathbf{S}_{\mathbf{d}}^{*} - \mathbf{S}_{\mathbf{m}})\right)}{\boldsymbol{\varphi}^{\mathbf{o}}\left(\mathbf{I}_2 \cdot \mathbf{S}_{\mathbf{m}} \cdot \mathbf{I}_2 - {}^{\mathbf{1}}/_{\mathbf{K_f}}\right) - \mathbf{I}_2 \cdot (\mathbf{S}_{\mathbf{d}}^{*} - \mathbf{S}_{\mathbf{m}}) \cdot \mathbf{I}_2}. \quad \text{(B-II)}$$

Here, $\otimes$ denotes the dyadic product, $\mathbf{S_m}$ is the compliance tensor of the solid mineral component (properties of mineral quartz were used in the case of sand-shale model), $\mathbf{S_d^*}$ is the effective compliance tensor for the dry sand-shale medium, and $\mathbf{S^*}$ is the effective compliance tensor for the saturated sand-shale medium. In Equation (B-II), φ^o is the total porosity and $\mathbf{I_2}$ is the (symmetric) identity matrix for second-rank tensors.

In the case of a composite porous medium that is partially saturated with oil, gas and water, K_f may be regarded as the bulk modulus of an effective fluid given by Wood - also known as the Reuss average (Mavko et al., 2009):

$$\frac{1}{K_f} = \frac{S_w}{K_w} + \frac{S_o}{K_o} + \frac{S_g}{K_g}, \quad \text{(B-III)}$$

where

$$S_w + S_o + S_g = 1. \quad \text{(B-IV)}$$

Here, S_w, S_o and S_g represent the saturation for water, oil and gas, and K_w, K_o and K_g represent the bulk modulus for water, oil and gas.